Meteorologische Zeitschrift, Vol. 23, No. 5, 491–510 (published online December 11, 2014)

The effect of soil moisture and atmospheric conditions on the development of shallow cumulus convection: A coupled large-eddy simulation–land surface model study

Andreas Chlond[1*], Otto Böhringer[1], Torsten Auerswald[2] and Frank Müller[3]

[1]Max Planck Institute for Meteorology, Hamburg, Germany
[2]Universität Tübingen, Umweltphysik, Tübingen, Germany
[3]NATO, SHAPE, NMR DEU, Belgium

(Manuscript received January 10, 2014; in revised form May 30, 2014; accepted July 10, 2014)

Abstract

Many processes and feedback mechanisms are involved in land-atmosphere interactions that play an important role in determining the boundary layer structure throughout the diurnal cycle. Here, the effect of soil moisture on the development of shallow cumulus convection is investigated using a coupled large-eddy simulation (LES)–land surface model (LSM) framework. First, the coupled model is run for an idealised case based on measurements at the ARM Southern Great Plain site on 21 June 1997 to demonstrate that many characteristics of the subcloud layer turbulence and of the cumulus layer can be modelled successfully. Moreover, an extensive sensitivity study is performed with different amounts of soil moisture and varying atmospheric conditions. Our results support the hypothesis that the response of shallow cumulus clouds due to a change of soil moisture severely depends on the thermal stability conditions. Furthermore, they also point out that the atmospheric moisture content is as important as the static stability in determining the boundary layer characteristics and in particular the fractional cloud cover. The results demonstrate that the soil moisture-cloud cover coupling is positive in most of the cases. However, we show that under specific conditions (a less stably stratified moist atmosphere) convective activity and cloud formation is stronger over dry soils, where the principle driving mechanism for cloud development is the boundary layer growth that tends to increase relative humidity by adiabatic cooling of the air at the top of the boundary layer. This leads to a soil moisture cloud cover relationship in which the cloud cover fraction decreases with an increase of soil moisture. Moreover, our findings suggest that in the limiting case of a water saturated soil the mean cloud cover is independent of static stability, but only depends on the vertical integrated atmospheric moisture content.

Keywords: land-atmosphere interaction, shallow cumulus clouds, diurnal cycle, coupled large-eddy simulation-land surface model

1 Introduction

The interactions between the land surface and the atmosphere play an important role in our climate system, as they regulate numerous processes on a wide range of temporal and spatial scales (e.g., Le Mone et al., 2000; Pielke, 2001; Koster et al., 2004; Betts and Dias, 2010). In this context soil moisture is a key factor, as it controls an important component of the hydrological cycle, namely the exchange of water between the surface and the atmosphere (e.g., Jacobs and de Bruin, 1992; Betts et al., 1996; Seneviratne et al., 2010). In particular, through the impact of soil moisture on the partitioning of the incoming solar and long-wave radiation in turbulent latent and sensible heat fluxes, soil moisture can influence several additional climate processes. These include air temperature and humidity, atmospheric boundary layer (ABL) turbulence, ABL entrainment and boundary layer thickness, formation of shallow clouds, and in some cases the initiation of deep convective precipitating clouds (e.g., Ek and Mahrt, 1994; Segal et al, 1995; Wetzel et al., 1996; Ek and Holtslag, 2004; van Heerwaarden et al., 2009; Hohenegger et al. 2009).

The connection between soil moisture and cloud development has been the focus of many studies on a wide range of time and space scales using a variety of methods including field and remote sensed observations (e.g., Findell and Eltahir, 1997; Koster et al., 2003; Findell and Eltahir, 2003a,b; Santanello et al., 2005, 2007, 2009; Cook et al., 2006; Taylor et al., 2007, 2011; Findell et al., 2011; Westra et al., 2012; Gentine et al., 2013), and models of different complexity. One-dimensional and mixed layer models have been used in many studies (e.g., Ek and Mahrt, 1994; Wetzel et al., 1996; Ek and Holtslag, 2004; van Heerwaarden et al., 2009, 2010) to investigate basic processes, mechanisms, and feedbacks involved in land-

*Corresponding author: Andreas Chlond, Max Planck Institute for Meteorology, KlimaCampus Hamburg, Bundesstr. 53, 20146 Hamburg, Germany, e-mail: andreas.chlond@mpimet.mpg.de

DOI 10.1127/metz/2014/0576

Gebrüder Borntraeger Science Publishers, Stuttgart, www.borntraeger-cramer.com

atmosphere interactions. Using this framework, Ek and Mahrt (1994) and Ek and Holtslag (2004) developed a simplified soil-boundary layer model and a method to analyse the relative humidity tendency at the top of the boundary layer (as an indicator for the chance of cloud formation) and demonstrated that atmospheric stratification above the boundary layer and soil moisture control boundary layer cloud development. Remarkably, a regime was identified in which the tendency of relative humidity at boundary layer top was found to increase with decreasing soil moisture content for sufficiently weak free atmospheric stability. Westra et al. (2012) recently were able to provide observational evidence for this regime using data from the African Monsoon Multidisciplinary Analysis measurement campaign. Recently van Stratum et al. (2014) proposed a new mixed-layer formulation and validated this model with large-eddy simulations from the ARM (see below) case. The mixed-layer model was driven with surface fluxes and was shown to successfully reproduce the processes that govern the shallow cumulus topped convective boundary layer. In particular, the model was able to reproduce the transition from clear to cloudy boundary layers and hence could correctly predict the timing of the onset of clouds. They were also able to explore the shallow cumulus parameter space by varying initial temperature, moisture content, and free tropospheric lapse rates of temperature and moisture.

On the other side of the complexity spectrum, regional and cloud resolving models (e.g., Pan et al., 1996; Hohenegger et al., 2009; Schlemmer et al., 2011) have been applied to investigate the relationships between soil moisture and precipitation associated with deep moist convection. Pan et al. (1996) studied the heavy rainfall event in 1993 in the mid-west of the United States using a regional weather model and found both negative and positive feedbacks between the soil moisture content and the amount of precipitation. Hohenegger et al. (2009) also found different signs of the soil moisture-precipitation feedback depending on whether the simulations allow an explicit treatment of convection or not. Schlemmer et al. (2011) employed an idealized cloud-resolving modelling framework and found that the stability of the atmosphere is a decisive factor determining the strength of convection and the timing and intensity of precipitation. Finally, in order to resolve the detailed turbulent motions and dynamics of scalars, momentum, and boundary layer cloud characteristics within the ABL, large-eddy simulation (LES) models have been applied (e.g., Golaz et al., 2001; Huang and Margulis, 2011) to study the local relationship between soil moisture and non-precipitating ABL clouds over a homogeneous land surface. Using an uncoupled LES model forced by sensible and latent surface fluxes Golaz et al. (2001) found nearly no change in cloud cover over dry relative to wet soils in their study. However, they found a large difference in structure and cloud development over wet and dry soils. Applying a coupled LES-land surface model (LSM), Huang and Margulis (2011) found that the cloud cover fraction increases with increasing soil moisture only in cases with strong atmospheric stability, and an opposite result has been found when weak atmospheric stability exists.

As seen from the review above, the soil moisture-cloud and precipitation coupling is a controversial subject (see also Seneviratne et al., 2010 and references therein). In order to further increase the understanding of these processes on boundary layer cloud development, a large-eddy simulation (LES) model coupled with a land surface model (LSM) is used. In the LES model the large-scale turbulent eddies are explicitly resolved while the effect of the less-energetic subgrid-scale turbulent eddies has to be parameterized. Previous studies have shown that this type of model provides realistic results if it is applied to simulate the development of cumulus clouds in the ABL (e.g., Neggers et al., 2002; Siebesma et al., 2003; Stevens, 2007; Stevens and Seifert, 2008). These studies clearly demonstrate that LES models are useful tools to study cumulus clouds to advance the understanding of the physical processes that determine the thermal and dynamical state of the cloud topped ABL.

The aim of this study is to investigate the influence of soil moisture on cloud development in the convective boundary layer at diurnal time scales and to evaluate the conceptual modelling framework of Ek and Mahrt (1994) and Ek and Holtslag (2004). In these studies two opposing effects that may influence the formation of boundary layer clouds have been identified and discussed. On the one hand, a greater soil moisture content results in boundary layer moistening, but, on the other hand, also leads to weaker surface sensible heat fluxes and to weaker boundary layer growth. As a result of these opposing effects, the net effect of soil moisture changes on the potential for boundary layer cloud development cannot be predicted with simple methods, but requires the application of a complex modelling framework. For this reason, we apply a coupled LES-LSM to reliably predict which of the above mentioned processes dominate as function of the soil moisture content and atmospheric conditions. Here, a model configuration consisting of the MPI-LES-model of Chlond (1992, 1994) and the Surface Energy and WAter Balance (SEWAB)-model developed by Mengelkamp et al. (1997, 1999, 2001) is used. With this coupled model configuration several simulations have been performed, where various parameters such as soil moisture content and profiles of temperature and humidity in the boundary layer have been changed systematically. Numerical simulations performed with this coupled model are based on an idealization of observations of a convective boundary layer made at the Southern Great Planes (SGP) site of the Atmospheric Radiation Measurement (ARM) program on 21 June 1997. During this day the diurnal evolution of a convective boundary layer with very weak large-scale forcing has been observed. Our study is strongly linked to the investigation of Huang and Margulis (2011), already mentioned above. Previous

work is extended by considering for the first time the combined influence of atmospheric humidity, static stability, and of soil moisture content on the sensitivity of shallow cumulus convection using a complex modelling framework. We investigate how the atmospheric humidity content among the two other main factors (namely, atmospheric stability and soil moisture content) controls the boundary layer cloud development. The importance of free-tropospheric humidity content and dry-air entrainment on the evolution of surface heat fluxes and the evolution of the ABL has been stressed by Santanello et al. (2007), Vilà-Guerau de Arellano (2007) and van Heerwaarden et al. (2010) who demonstrated that in certain conditions the evolution of surface fluxes, relative humidity, and ABL height can be as sensitive dependent on free tropospheric moisture conditions as to land-surface properties. Also Derbyshire et al. (2004) have already recognized the significance of mid-tropospheric humidity on moist convection. Their modelling study suggests a significant impact of different moisture conditions on the development of moist convection. The most striking result was that a dry-tropospheric moisture profile can suppress deep convection in favour of a shallow convection regime.

The paper is organized as follows. In section 2 the models used are described, while in section 3 a brief overview of the experimental design is given. This includes the description of the setup of the case study, which is used as reference simulation, and of the sensitivity study. Section 4 briefly summarises the main characteristics of the reference simulation before presenting the results of the sensitivity study. The impact of soil moisture content and of the thermodynamic atmospheric conditions on the simulated boundary layer structure is analysed and discussed. To interpret and understand our results, we apply a diagnostic method that allows us to quantify the strength of the different processes by an analysis of the individual contributions to the tendency of the relative humidity at the top of the mean cloud layer. Finally, section 5 summarizes the conclusions drawn in this work.

2 Models

Over the past three decades, LES has become one of the leading methods to advance our understanding of processes in the planetary boundary layer. The fundamental approach of LES is to explicitly resolve large turbulent eddies which contain most of the turbulent kinetic energy and are responsible for most of the turbulent transport. The basic dynamical framework employed here is the MPI-LES model which has been described in Chlond (1992, 1994). The model takes into account most of the physical processes occurring in the moist boundary layer including the effects of subgrid-scale (SGS) motions. The SGS model is based on a transport equation for the SGS turbulent kinetic energy (Deardorff, 1980).

To simulate land surface and soil processes, the Surface Energy and WAter Balance SEWAB-model developed by Mengelkamp et al. (1997, 1999, 2001) is used. It solves the diffusion equations for heat and moisture on a multi-layer grid in a vertical column of soil between the lower soil surface and the atmosphere including the effect of vegetation. Boundary conditions at the upper interface in terms of short- and longwave radiative fluxes as well as atmospheric near surface values for temperature, moisture content, and wind speed have to be provided. The LSM is run using six layers with a total depth of 2.3 m. The moisture flux at the surface is calculated as the weighted average of the moisture flux from bare surfaces and of the evapotranspiration from vegetated surfaces. Soil and vegetation type as well as the fraction of a grid square covered by vegetation have to be prescribed. The values for soil properties and vegetation related parameters are taken from look-up tables given by Mengelkamp et al. (1997). In contrast to Vilà-Guerau de Arellano et al. (2012) who explored an example of a biogeophysical feedback operating on long time scales and revealed that boundary layer clouds may be suppressed by plants in a warming CO_2-rich atmosphere, our model treats evapotranspiration from low vegetation using a resistance approach that allows the extraction of water from the upper soil layer only. The vegetation does not experience any additional stress due to limited radiation or rising atmospheric CO_2 concentrations. Nevertheless, we are of the opinion that our main findings still remain valid because our study concentrates on the investigation of the short-term, diurnal evolution of the atmospheric boundary layer-soil system where evaporation is limited by the soil moisture content and not by the available surface energy.

Coupling to the LES model is achieved through a surface energy budget which partitions the available radiative forcing into ground heat flux and sensible and latent heat fluxes. Assuming that no heat is stored at the surface, the energy balance equation for the skin layer may be written as

$$R_{\mathrm{swd}}\cdot(1-a)+\varepsilon\cdot(R_{\mathrm{lwd}}-\sigma\cdot T_{\mathrm{s}}^4)+H+L\cdot E-\Lambda\cdot(T_{\mathrm{s}}-T_{\mathrm{d}})=0, \tag{2.1}$$

where R_{swd} and R_{lwd} represent downward short-wave and long-wave radiation at the surface, a is the albedo, ε is the surface emissivity and σ the Stefan-Boltzmann constant, T_{s} is the temperature of the surface, H and E are the heat flux and the moisture flux, L is the latent heat of evaporation, and $\Lambda\cdot(T_{\mathrm{s}}-T_{\mathrm{d}})$ is the soil heat flux into a deeper layer with temperature T_{d}, using a conductivity Λ. The LES model provides the downwelling radiative fluxes at the surface and the atmospheric state variables at the lowest grid level as forcing for the LSM. To calculate the radiative fluxes a very simple approach is adopted. The short-wave radiation R_{swd} is assumed to depend on the radiation for a cloudless sky and a factor depending on the cloud cover as described in Mengelkamp et al. (1999) to account for feedbacks of cloud cover on incoming solar radiation. The downward

long-wave radiation flux emitted from the atmosphere, R_{lwd}, is parameterized according to Deardorff (1978). Eq. (2.1) is then solved iteratively for T_{s} to calculate the turbulent surface heat fluxes for which a resistance formulation is applied to include the effects of the land surface properties on the exchange of heat and moisture. These turbulent fluxes are used as lower boundary conditions for the LES model to update the atmospheric state. In this way the two-way interaction between the land and the overlying atmosphere is captured. The skin layer is coupled to a five layer soil scheme to advance the soil temperature and moisture content in time according to the governing equations of energy and water conservation. More details about the formulation of the surface fluxes and the coupling strategy can be found in Mengelkamp et al. (1999). General principles of the method for coupling land surface schemes to the atmosphere were presented by Best et al. (2004).

Since we use a simple modelling approach to calculate the radiative fluxes we cannot investigate the influence of cloud shading from a broken cloud layer at top of a convective boundary layer. This requires the application of a more sophisticated radiation scheme that allows us to calculate a local surface radiation budget in response to cloud induced heterogeneity, which is beyond the scope of this paper. Moreover, since that largest effect of shadows on convection is expected to occur in situations with weak mean wind (Schumann et al., 2002) we expect that the conclusions drawn in our study remain valid despite the simple modelling approach adopted. Results obtained by Lohou and Patton (2014) indicate, however, that the turbulence structure of the boundary layer may change noticeably due to cloud-induced surface heterogeneities, which may justify refined studies in the future.

The runs with the coupled model use a computational domain of size $12.8 \times 12.8 \times 4.4\,\mathrm{km}^3$. Double-periodic lateral boundary conditions are employed. At the upper boundary a Rayleigh damping sponge layer starting at a height of 4 km is used to damp gravity waves. The first simulation for the reference case (see below) was carried out with grid intervals of $\Delta x = \Delta y = 50\,\mathrm{m}$ and $\Delta z = 40\,\mathrm{m}$. A second, lower horizontal resolution simulation was performed with a grid spacing of 100 m in the horizontal directions and 40 m in the vertical. A time step of 1 s was used for both runs. Results from those two experiments agreed well with each other, indicating that the model results are robust with respect to variations in the horizontal resolution. Nevertheless, we retained a higher resolution for all other additional experiments.

3 Case description and model setup

To investigate the soil moisture-cloud feedback, we consider a set of simulations of the (semi-) diurnal variation of the convective boundary layer over land. The set consists of one reference simulation and a number of sensitivity experiments. The setup for the reference simulation is based on a single-day case using measurements taken during the development of shallow cumulus convection observed at the SGP site of the ARM program near Lamont, Oklahoma, on 21 June 1997. These data correspond to a case of daytime, non-precipitating cumulus clouds over land developing on top of an initially clear convective boundary layer. This case has already been intensively studied in the 6$^{\mathrm{th}}$ Global Energy and Water Cycle Experiment (GEWEX) Cloud System study (GCSS) model intercomparison project to test the ability of LES models to simulate the development of shallow cumulus over land, provided that the time varying surface fluxes and the large-scale forcings are given. The basic characteristics of the case are described here, but more specific information on the project and a detailed specification of the case is provided in Brown et al. (2002).

To configure the coupled model for the reference run both sub-models, the LES model and the LSM are in a first step run in an uncoupled forced mode. This procedure is required in order to specify the initial soil moisture content. The case consists of a 12.5-hour simulation starting at 11:30 UTC (corresponding to 5:30 h local time), shortly after sunrise, with prescribed initial profiles, time dependent surface fluxes, large-scale advective forcings, and radiative tendencies. The initial and boundary conditions are based on observations and were specified in the form of simplified profiles. The initial setup of the LES-model is identical to the one used for the 6$^{\mathrm{th}}$ GCSS intercomparison project. All initial fields are set horizontally homogeneous at the beginning of the simulation except for random temperature perturbations which were imposed at each grid point in the lowest 200 m (with a maximum amplitude of 0.1 K at the surface decreasing linearly from that value to zero at 200 m) in order to initiate turbulence. A height independent large-scale horizontal pressure gradient was applied, equivalent, with a Coriolis parameter of $8.5 \times 10^{-5}\,\mathrm{s}^{-1}$ (corresponding to a latitude of 36 ° N), to a geostrophic wind of $U_{\mathrm{g}} = 10\,\mathrm{m\,s}^{-1}$ and $V_{\mathrm{g}} = 0\,\mathrm{m\,s}^{-1}$. The initial horizontal wind components (u, v) were set to $(U_{\mathrm{g}}, V_{\mathrm{g}})$ at all levels. Surface pressure was set to 970 hPa. Simplified profiles of liquid water potential temperature and total water mixing ratio were used as initial conditions for the thermodynamic variables. The potential temperature starts from a value of 299 K at the land surface and piecewise linearly increases up to 2500 m, where the lapse rate above is set to a constant value of $9.7\,\mathrm{K\,km}^{-1}$. Similarly, total water mixing ratio piecewise linearly decreases from a value of $15.2\,\mathrm{g\,kg}^{-1}$ at the ground to 2500 m, where the mixing ratio is set to a constant value of $3.0\,\mathrm{g\,kg}^{-1}$. Throughout this study this setup for the atmospheric variables will be referred to as "standard atmospheric setup". As already mentioned, the specification of the time series of the imposed surface fluxes which are used as lower boundary conditions to drive the LES model and the details of the

Table 1: Soil, vegetation, and surface parameters for model runs

Parameter	Type or value
Soil type	Silty clay loam
Volumetric water content at wilting point	0.2181 m^3m^{-3}
Volumetric water content at field capacity	0.3220 m^3m^{-3}
Volumetric water content at saturation	0.4700 m^3m^{-3}
Vegetation type	Short grass lands
Vegetation fraction	0.6
Leaf area index of vegetated surface fraction	1
Minimum/Maximum stomatal resistance	300 s m^{-1}
Albedo	0.17
Roughness length	0.035 m

representation of the effects of large-scale advection and radiation are given in Brown et al. (2002).

The results from the above described constrained LES run are used to generate the upper boundary conditions for the LSM in the uncoupled forced mode. Time varying fields of temperature, mixing ratio, horizontal wind speed, and radiative fluxes at the lowest computational level of the LES model are used to drive the LSM. We assume a homogeneous flat soil surface that is partially vegetated. A fraction of vegetation of 60 % is adopted. For the soil dependent parameters we adopt those for "silty clay loam", and for the vegetation dependent parameters the values for short grass lands are used. The short-wave albedo is set to 0.17 which is in the range of reported values (Duchon and Hamm, 2005), and the surface roughness length is set to 0.035 m (a characteristic value for the ARM site). A summary of the principal soil, vegetation, and surface parameters used in the LSM are listed in Table 1. Soil temperatures are initialized to be equal to the air temperature in the upper two layers (i.e., at $z = 0.025$ m, and $z = 0.125$ m), and a linear transition to a climatological value of 289.13 K in the fifth level at $z = 1.05$ m is imposed. With respect to the initial soil moisture profile, a linear relation between the upper layer at $z = 0.025$ m with a specified soil water content η and the maximum soil water content η_s of the given soil volume at $z = 1.05$ m is assumed. It turns out that a good match between calculated time dependent sensible and latent heat fluxes, respectively, and observed ones can be achieved with an initial volumetric soil moisture content of 0.3337 m^3/m^3, which corresponds to a saturation ratio $\sigma = \eta/\eta_s$ of 0.71, i.e., to 71 % of the maximum soil water content η_s. Using this value for the initial saturation ratio, the surface heat fluxes calculated by the coupled LES-LSM are found to be close to the observed ones and hence close to the surface fluxes that we prescribed as lower boundary conditions for the LES model run in the uncoupled constrained mode (see section 4). As in our study, Lohou and Patton's (2014) simulated case is based on observations from the ARM SGP central facility on 21 June 1997. However, between our study and Lohou and Patton's (2014) work there exist some differences in the specification of initial values of surface parameters like

Table 2: Main characteristics of the different simulation sets. Each set consists of sixteen simulations with soil moisture saturation ratios between $\sigma = 0.25$ and saturation (i.e., $\sigma = 1.0$) with an interval of 0.05 between successive simulations.

Name of simulation set	Temperature profile	Humidity profile
STD	standard	standard
L_STABLE	less_stable	standard
M_STABLE	more_stable	standard
STD_DRY	standard	dry
STD_MOIST	standard	moist
STD_DRY_FA	standard	dry_free_atm
STD_MOIST_FA	standard	moist_free_atm
L_STABLE_DRY	less_stable	dry
L_STABLE_MOIST	less_stable	moist
L_STABLE_DRY_FA	less_stable	dry_free_atm
L_STABLE_MOIST_FA	less_stable	moist_free_atm
M_STABLE_DRY	more_stable	dry
M_STABLE_MOIST	more_stable	moist
M_STABLE_DRY_FA	more_stable	dry_free_atm
M_STABLE_MOIST_FA	more_stable	moist_free_atm

the surface roughness (0.035 m vs. 0.08 m), albedo (0.17 vs. 0.20), the soil moisture content (0.334 m^3m^{-3} vs. 0.363 m^3m^{-3}) etc. At first glance, this appears strange if one takes into account that both simulations try to reproduce the surface fluxes observed at the ARM SGP site. However, it is worth noting that in both studies different complex model systems are used that differ in the radiation model (that determines the available energy), in the LES model (which determines the turbulence structure of the cloud topped boundary layer), and in the LSM (which determines the partition of available energy into the turbulent sensible and latent heat fluxes and the ground heat flux). Keeping this in mind, it appears reasonable that the parameter combinations generating the best agreement between the simulated surface fluxes and the surface flux measurements are not identical, but differ from each other within certain limits. Finally, we note that our simulated fluxes fit Brown et al. (2002) specifications of the surface heat and moisture fluxes better than those of Lohou and Patton (2014).

In addition to the reference run we have performed 240 sensitivity experiments with the coupled LES-LSM. These experiments are obtained by simultaneously modifying, at the initial time, the soil water content, the thermal stratification, and the atmospheric moisture profile. We performed fifteen sets (see Table 2) of simulations with three different liquid water potential temperature profiles and five different total water mixing ratio profiles. Each set consists of sixteen simulations with soil moisture saturation ratios between $\sigma = 0.25$ and saturation (i.e., $\sigma = 1.0$) with an interval of 0.05 between successive simulations. To investigate the role of thermal stratification for land-atmosphere interaction, three cases (*standard, less_stable, more_stable*) were performed for each soil moisture saturation ratio value. The case *less_stable* has a weaker ther-

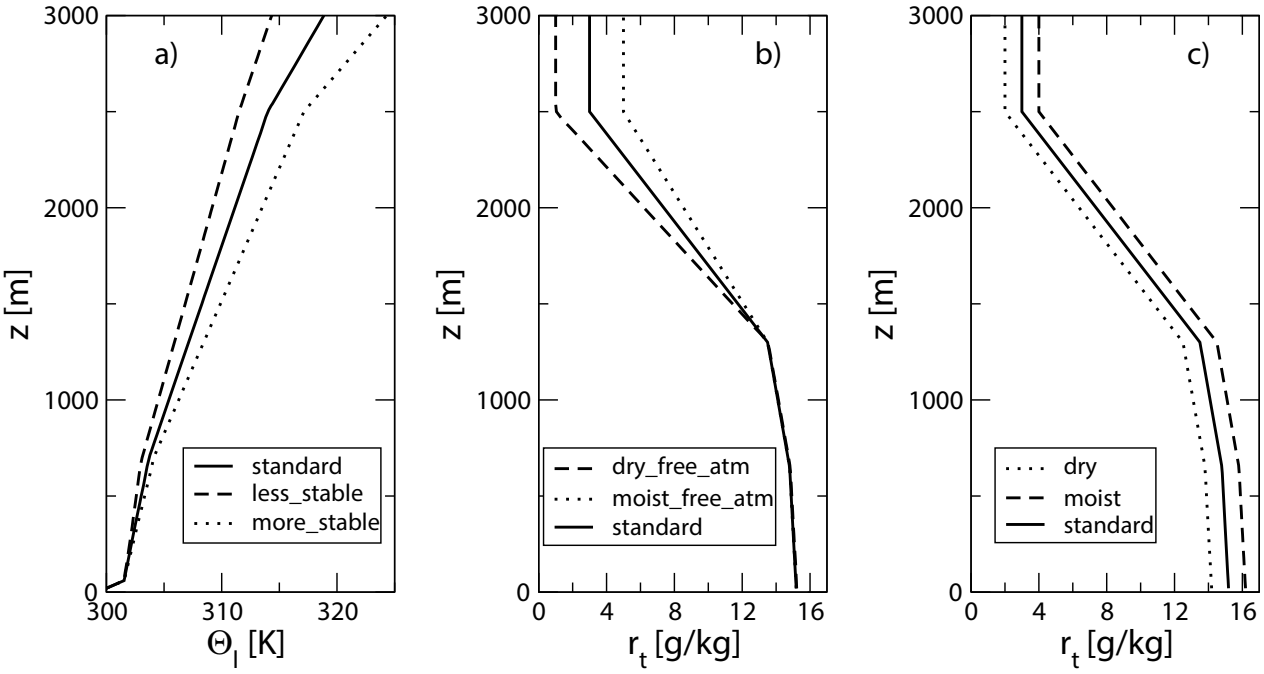

Figure 1: Initial profiles of (a) liquid water potential temperature θ_l and (b+c) total water mixing ratio r_t. Solid lines mark the *standard* profiles used in the reference run. In (a) the dashed line represents the *less_stable* case, and the dotted line represents the *more_stable* profile. In (b) dashed and dotted lines refer to the profiles *dry_free_atm* and *moist_free_atm*, respectively. In (c) dashed line and dotted lines refer to the *dry* and *moist* total water mixing ratio profiles, respectively.

mal stratification (i.e., less stable with lapses rates of $(d\theta/dz)_{\mathrm{ABL}} = 4.7\,\mathrm{K\,km^{-1}}$ within the bulk of the ABL and $(d\theta/dz)_{\mathrm{FA}} = 5.7\,\mathrm{K\,km^{-1}}$ in the free atmosphere above 2500 m, respectively) compared to the *standard* case (with lapse rates of $(d\theta/dz)_{\mathrm{ABL}} = 5.7\,\mathrm{K\,km^{-1}}$ and $(d\theta/dz)_{\mathrm{FA}} = 9.7\,\mathrm{K\,km^{-1}}$, respectively), and the third *more_stable* case has a stronger thermal stability (i.e., more stable with lapse rates of $(d\theta/dz)_{\mathrm{ABL}} = 7.2\,\mathrm{K\,km^{-1}}$ and $(d\theta/dz)_{\mathrm{FA}} = 14.4\,\mathrm{K\,km^{-1}}$, respectively) compared to the standard profile. To test the response of the model to a changed humidity in the boundary layer and the lower troposphere, for each temperature profile above, additional sets with runs are performed, where also the humidity profile has been modified. The atmospheric moisture profiles applied in the simulations are denoted by *dry*, *moist*, *dry_free_atm* and *moist_free_atm*. The case *dry* refers to a total water mixing ratio profile that has been shifted by $-1\,\mathrm{g\,kg^{-1}}$ relative to the standard profile, and the *moist* case utilizes a humidity profile, where the standard profile is shifted by $+1\,\mathrm{g\,kg^{-1}}$. The atmospheric moisture conditions *dry_free_atm* and *moist_free_atm* refer to cases with total water mixing ratio profiles which remain unchanged relative to the standard profile below 1300 m, but have been modified in layers above 1300 m by changing the total water mixing ratio at 2500 m and above to $r_{\mathrm{t,top}} = 1\,\mathrm{g\,kg^{-1}}$ and to $r_{\mathrm{t,top}} = 5\,\mathrm{g\,kg^{-1}}$, respectively. Between 1300 m and 2500 m linear interpolation was used to obtain values at intermediate levels.

In total fifteen simulation sets are generated (according to the number of combinations resulting from three temperature profiles and five humidity profiles) which are named

- STD, L_STABLE, M_STABLE
- STD_DRY, STD_MOIST, STD_DRY_FA, STD_MOIST_FA
- L_STABLE_DRY, L_STABLE_MOIST, L_STABLE_DRY_FA, L_STABLE_MOIST_FA
- M_STABLE_DRY, M_STABLE_MOIST, M_STABLE_DRY_FA, M_STABLE_MOIST_FA

The initial profiles of liquid water potential temperature θ_l and total water mixing ratios r_t adopted in the reference and the sensitivity simulations are displayed in Fig. 1 with different line patterns. An overview over the different simulation sets used in the sensitivity analysis is given in Table 2.

4 Results

4.1 Reference run

First, the results of the reference simulation are presented to review the performance of the coupled model for the ARM case. In the reference run the coupled LES-LSM starts at 11:30 UTC (corresponding to 5:30 h local time) with the standard atmospheric setup described in section 3, with an initial soil moisture saturation ratio $\sigma = \eta/\eta_s$ of 0.71 (corresponding to an initial volumetric soil moisture content of $\eta = 0.3337\,\mathrm{m^3 m^{-3}}$), and lasted for 12.5 hours. Note, that in the coupled mode

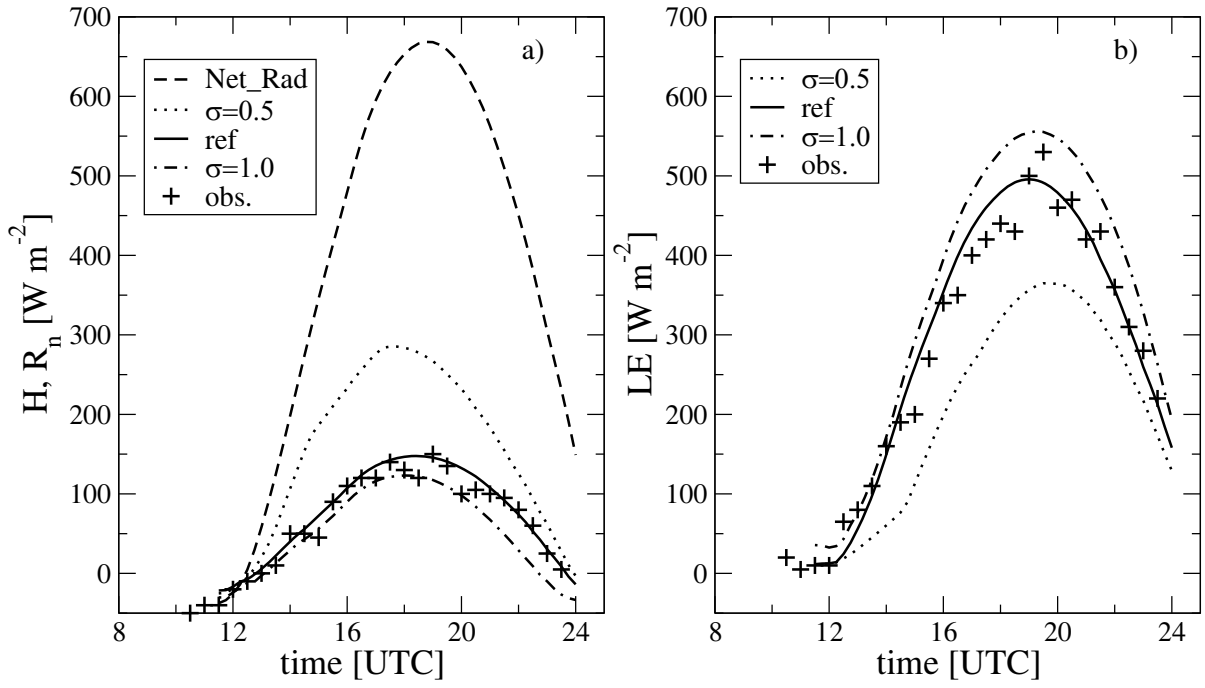

Figure 2: Time series of area averaged (a) surface sensible heat flux H (solid line) and net radiation R_n (dashed line), and (b) latent heat flux LE (solid line), as simulated with the coupled model in the reference run. Observed fluxes are indicated by crosses and are based on measurements taken on 21 June 1997 at the central facility of the ARM-Project in Lamont, Oklahoma, as reported by Brown (2002). In addition, time series of sensible and latent surface fluxes of simulations from the set STD which utilize a soil saturation ratio of $\sigma = 0.5$ and $\sigma = 1.0$, respectively, are additionally plotted for comparison.

the LSM provides the lower boundary conditions for the LES model. The SEWAB model calculates the surface sensible and latent heat fluxes for every soil column driven by the atmospheric variables delivered by the LES model. First, the general development of the simulation is discussed. We will concentrate on surface fluxes, the evolution of mean profiles, and on the growth and decay of cumulus clouds. Next, we consider the turbulence structure of the convective boundary layer (before cloud formation) and of the cloud topped boundary layer (after cloud formation).

Time series of area averaged (a) surface sensible heat flux H and net radiation R_n, and (b) surface latent heat flux LE are displayed in Fig. 2. The net radiative flux resembles a typical diurnal cycle, starting with 0 W m^{-2} at 12:00 UTC (06:00 h local time) and attaining a maximum value of about 650 W m^{-2} at 19:00 UTC (13:00 h local time). It can be seen that the model estimates for the surface fluxes are in good agreement with the measured data collected at the SGP central facility. The strong diurnal cycle is clearly identifiable with maximum values of sensible and latent heat fluxes of 150 W m^{-2} and 500 W m^{-2}, respectively. The typical Bowen ratio is about 0.3 for the reference case. Moreover, to illustrate the sensitivity of the partitioning of the available energy into sensible and latent heat fluxes with respect to the initial soil moisture content, time series of sensible and latent surface fluxes of simulations from set STD which utilize a soil saturation ratio of $\sigma = 0.5$ and $\sigma = 1.0$, respectively, are additionally plotted for comparison. As expected, the surface evaporation decreases (increases) and the surface sensible heating increases (decreases) for drier (moister) soils, respectively. In our simulations the reduction in the soil water content during the course of the integrations is significant, but is rather small as the loss of water is less than 20 %.

Fig. 3 shows the temporal development of area averaged vertical profiles of (a) the liquid water potential temperature $\langle\theta_l\rangle$ and (b) the total water mixing ratio $\langle r_t\rangle$ at different times from the reference simulation. As expected, the boundary layer grows, warms, and moistens through the day producing a well mixed layer in which nearly no vertical gradient of liquid water potential temperature and total water mixing ratio occurs. In Fig. 4 the simulated evolution of (a) total cloud cover, which is defined as the fraction of the vertical columns that contain cloud water, (b) mean cloud base height and mean cloud top height, and (c) liquid water path are displayed. Cloud development starts around 16:00 UTC (10:00 h local time). After this time the cloud base rises slowly with time from around 750 m at 16:00 UTC to 1400 m at 24:00 UTC. This increase of cloud base height with time is consistent with the warming of the subcloud layer shown in Fig. 3. Cloud-top growth is steady and rather fast during the initial growth phase of cloud development. A maximum cloud top height of 2900 m is reached at around 21:30 UTC, about five and a half hours after initial cloud formation. The largest cloud fraction occurs early within the initial growth phase at around 18:00 UTC with a maximum value of around 26 % total

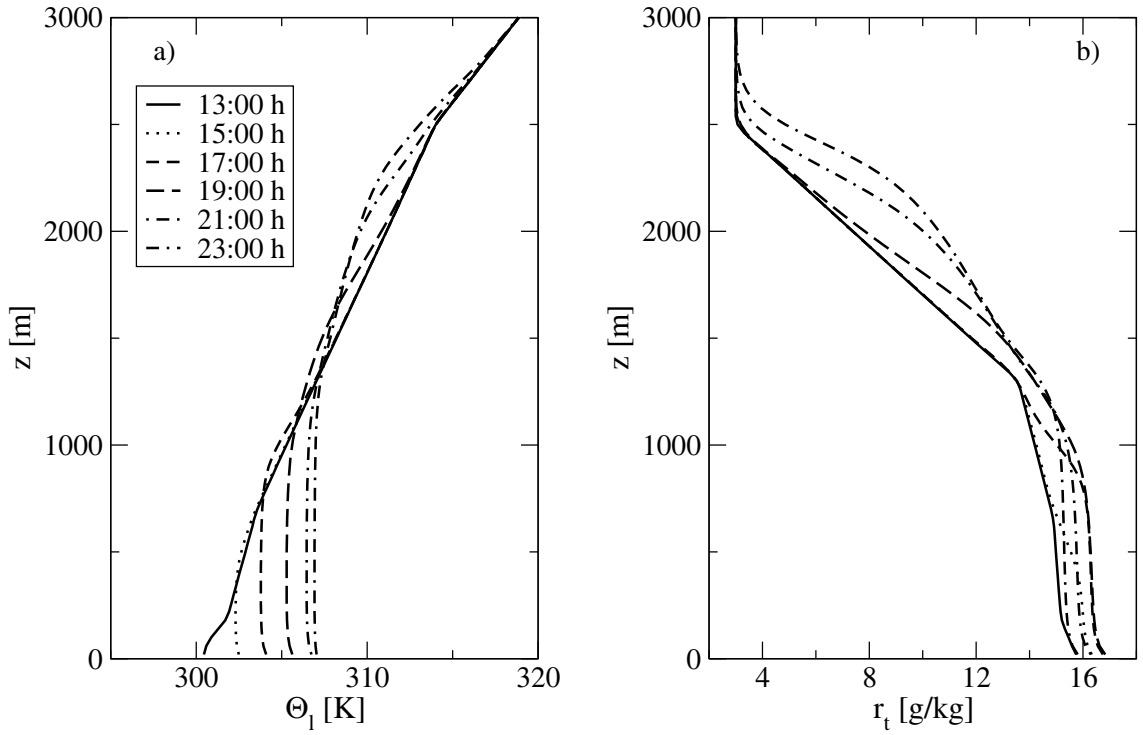

Figure 3: Temporal development of area averaged vertical profiles of (a) the liquid water potential temperature $\langle\theta_l\rangle$ and (b) the total water mixing ratio $\langle r_t\rangle$ at different times from the reference simulation. Legend explains the various line patterns used in the plot. Profiles are one-hour averaged, centred at the displayed times.

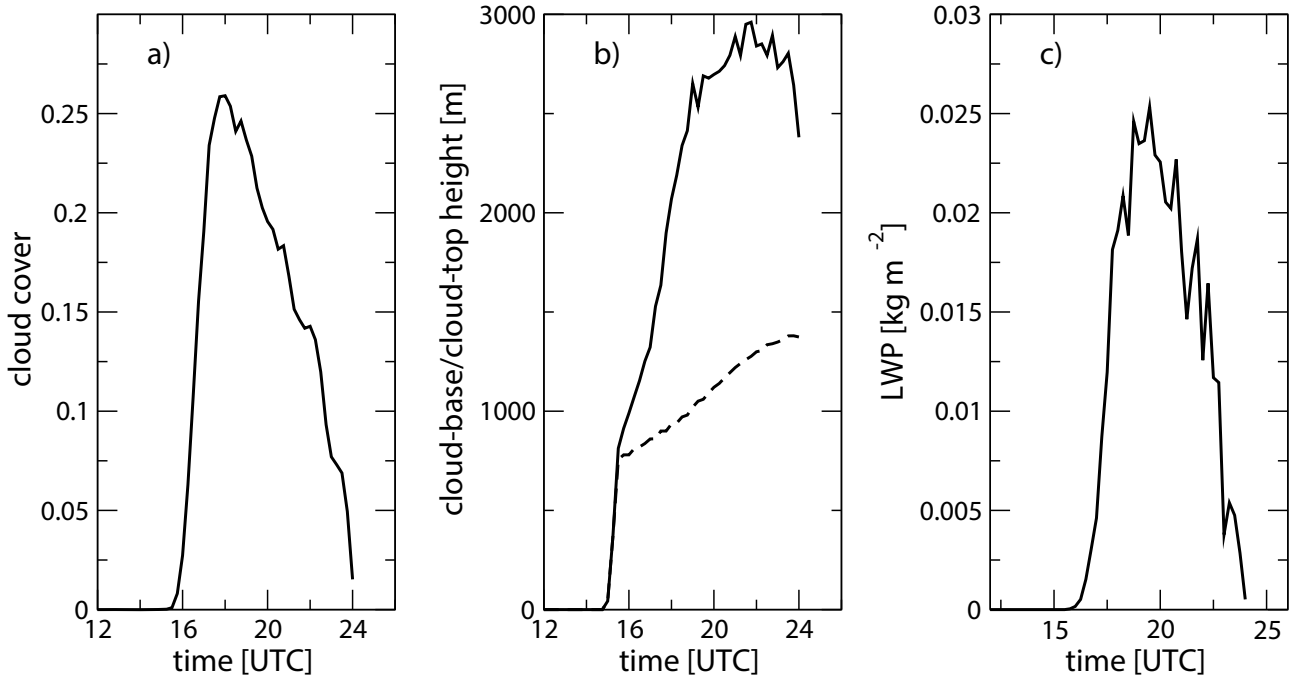

Figure 4: Time series (smoothed over one hour) of (a) total cloud cover, (b) mean cloud base height (dashed line) and mean cloud top height (solid line), and (c) liquid water path, respectively, from the reference simulation.

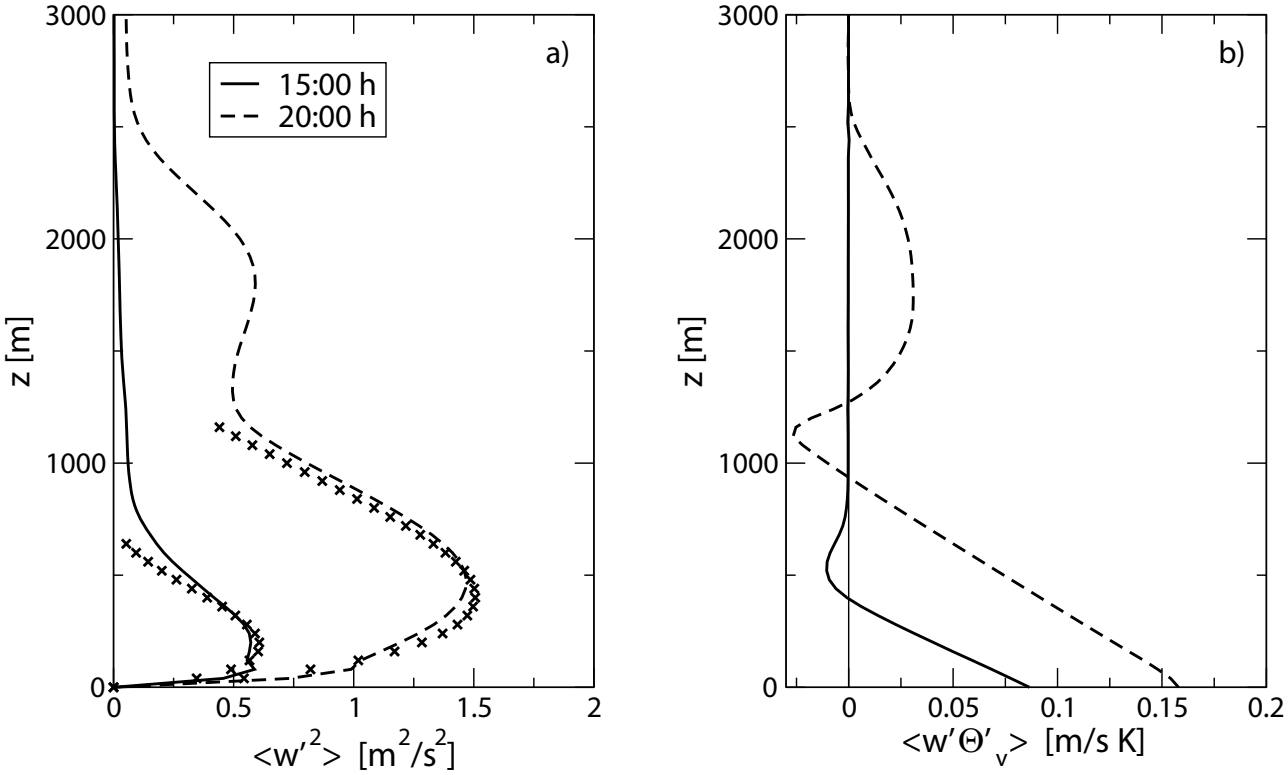

Figure 5: Profiles of 1-h averaged total (resolved plus subgrid-scale) (a) vertical velocity variance $\langle w'^2 \rangle$ and (b) the total buoyancy flux $\langle w'\theta'_v \rangle$, centred at 15:00 UTC (solid lines) and 20:00 UTC (dashed lines), respectively, from the reference simulation. The crosses in (a) show the function $\langle w'^2 \rangle = 1.8(z/z_i)^{2/3}(1 - 0.8z/z_i)^2 w_*^2$ (Lenschow et al. 1980). Here z_i denotes the depth and w_* is the velocity scale of the convective boundary layer at 15:00 UTC and of the subcloud layer at 20:00 UTC, respectively (see also text).

cloud cover. After 18:00 UTC cloud fraction slowly declines before falling away quite sharply as surface forcing decays. Values of area averaged liquid water path are relatively low with maximum values of 0.025 kgm^{-2} occurring around 20:00 UTC.

This paragraph gives basic results of the simulated total (resolved plus subgrid-scale) vertical velocity variance $\langle w'^2 \rangle$ and the total buoyancy flux $\langle w'\theta'_v \rangle$. Fig. 5 shows that marked differences exist in the turbulence structure during the time before cloud formation (at 15:00 UTC) and after cumulus clouds have formed (at 20:00 UTC). At 15:00 UTC the boundary layer has a depth – based on the height of the minimum of the buoyancy flux – of $z_i = 500\,\mathrm{m}$. Together with the simulated surface buoyancy flux this gives a convective velocity scale value of about $w_* = 1\,\mathrm{m\,s}^{-1}$, while the friction velocity scale u_* is around $0.6\,\mathrm{m\,s}^{-1}$. This results into a stability parameter $-z_i/L$ (where L denotes the Monin-Obukhov length) of around 2. Observations (e.g., Nicholls and Readings, 1979; Grant, 1986) suggest that even at these moderate levels of instability the vertical velocity variance should scale convectively. It is therefore logically consistent to find a good agreement between our LES model results and the best fit to the free convective data of Lenschow et al. (1980), and confirms similar results obtained by Brown et al. (2002). At 20:00 UTC, after cumulus clouds have formed, the vertical velocity exhibits now two maxima, one in the subcloud layer and a secondary maximum in the cloud layer. Nicholls and Le Mone (1980) demonstrated that despite the presence of clouds, convective boundary layer scaling should still be applicable in the subcloud layer. To test this hypothesis, we take z_i to be the height of the buoyancy flux minimum which occurs close to cloud base, then we have $z_i = 1200\,\mathrm{m}$, $w_* = 1.8\,\mathrm{m\,s}^{-1}$, $u_* = 0.6\,\mathrm{m\,s}^{-1}$, and $-z_i/L = 9$. This is sufficiently unstable for the vertical velocity variance to scale convectively. From Fig. 5 it can be seen that the LES results for $\langle w'^2 \rangle$ in the subcloud layer are, as already shown by Brown et al. (2002), consistent with well-established convective boundary layer scalings. The secondary maximum of $\langle w'^2 \rangle$ higher up is related to the cumulus activity in the cloud layer. The buoyancy flux profile at 20:00 UTC exhibits an almost linear decrease through the subcloud layer with a value at the top (corresponding to the cloud base height) which is of the order of −0.15 times the surface buoyancy flux. At 20:00 UTC a broad maximum of $\langle w'\theta'_v \rangle$ occurs in upper layers which is related to cumulus activity.

To summarize, this section is about the evaluation of the reference simulation. We find that the results shown above are broadly consistent with local surface measurements and with those obtained in connection with the sixth intercomparison case of GCSS Working Group 1 which have been elaborately discussed in Brown et al. (2002).

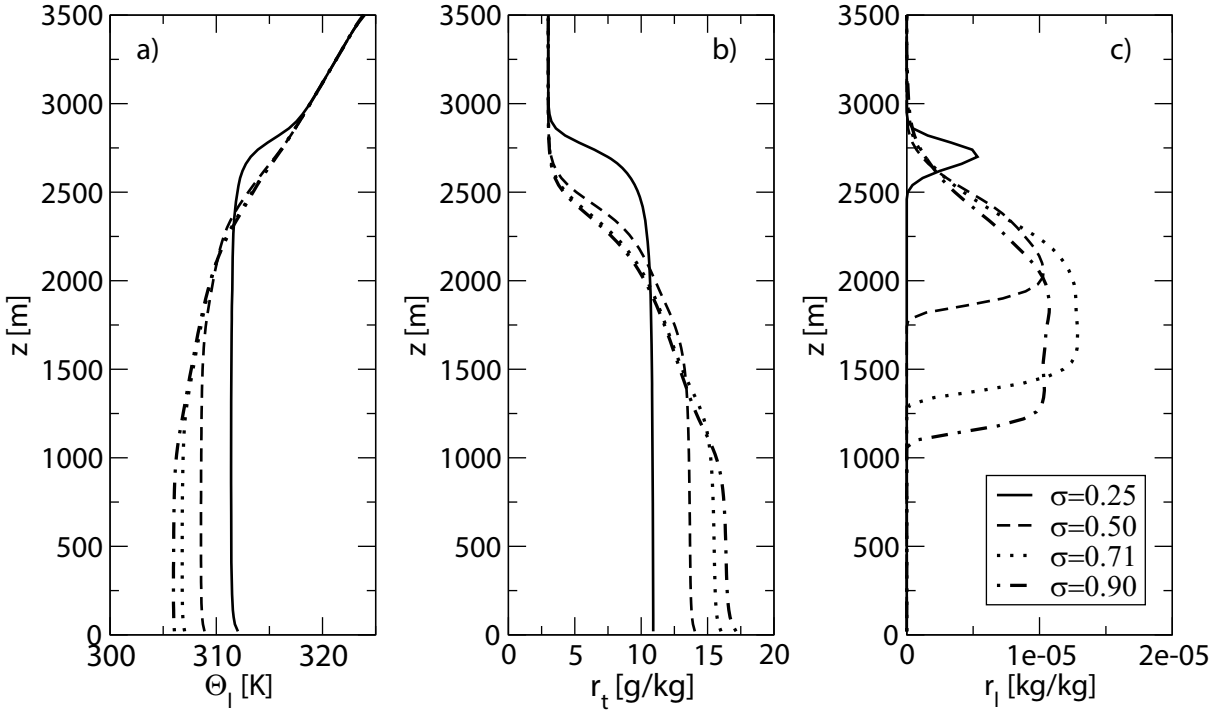

Figure 6: Vertical profiles of domain averaged (a) liquid water potential temperature $\langle\theta_l\rangle$, (b) total water mixing ratio $\langle r_t\rangle$, and (c) liquid water mixing ratio $\langle r_l\rangle$. Solid, dashed, dashed-dotted, and dotted lines are results for different soil moisture contents from the simulation set STD and the reference simulation. All profiles are 1-h averaged centred at 22:00 UTC.

4.2 Sensitivity runs

4.2.1 Effect of soil moisture content

To study the effect of soil moisture content on the development of shallow cumulus clouds, several model runs are conducted, where the initial soil moisture saturation ratio σ has been specified in the range between 0.25 and 1.

Fig. 6 shows domain averaged vertical profiles (1-h averaged) of (a) liquid water potential temperature $\langle\theta_l\rangle$, (b) total water mixing ratio $\langle r_t\rangle$, and (c) liquid water mixing ratio $\langle r_l\rangle$ from the reference run and for simulations from set STD centred at 22:00 UTC (16:00 h local time). In general, the profiles of $\langle\theta_l\rangle$ and $\langle r_t\rangle$ reflect the structure of a convective boundary layer, i.e., well-mixed profiles between the surface and the entrainment zone, where stronger gradients of liquid water potential temperature and total mixing ratio occur. It can be seen that due to the larger sensible heat flux over drier soils the boundary layer is warmed much stronger compared to the cases that start with a wetter soil. The larger sensible heat flux also results in a faster boundary layer growth. As a consequence, the top of the boundary layer is higher over drier soils compared to the boundary layer height over wetter soils at 22:00 UTC. Moreover, as can been seen in Fig. 6(c), the cloud base heights decrease with increasing soil moisture content and a shallower cloud layer develops over dry soil than over wet soil. The profiles of total water mixing ratio indicate that the boundary layer over dry soils is less humid than over wet soils, because the input of water vapour into the ABL is less over dry soils than over wet soils. This is illustrated in Fig. 7, where 1-hr averaged vertical profiles of the total (resolved plus subgrid-scale) turbulent moisture fluxes $\langle w' r_t'\rangle$ centred at 19:00 UTC (13:00 h local time) are shown. As we have already mentioned, the moisture flux near the surface increases with rising soil moisture content. In the upper part of the boundary layer the mixing of dry air from the free atmosphere into the boundary layer becomes important. It turns out that the entrainment flux is stronger over dry soils compared to wet soils, as more vigorous turbulent motions drive entraining eddies that incorporate free-tropospheric dry air into the ABL. This is reasonable because in the simplest case the entrainment velocity in the convective boundary layer is proportional to the surface sensible heat flux (e.g., Tennekes, 1973; van Zanten et al., 1999). As a consequence, the entrainment velocity and hence the boundary layer growth is faster over dry soil than over wet soil because the decomposition of the total available energy, which is given by the net radiation, into the surface evapotranspiration and the surface sensible heat flux depends on the soil moisture content (see Fig. 2). This feature is also visible in Fig. 12 where, among other quantities, the contribution of the boundary layer cooling to the total relative humidity tendency is displayed. This quantity is proportional to the mean boundary layer growth and monotonously (depending on the static stability) increases with decreasing soil moisture content indicating that the boundary layer growth increases with decreasing soil moisture content.

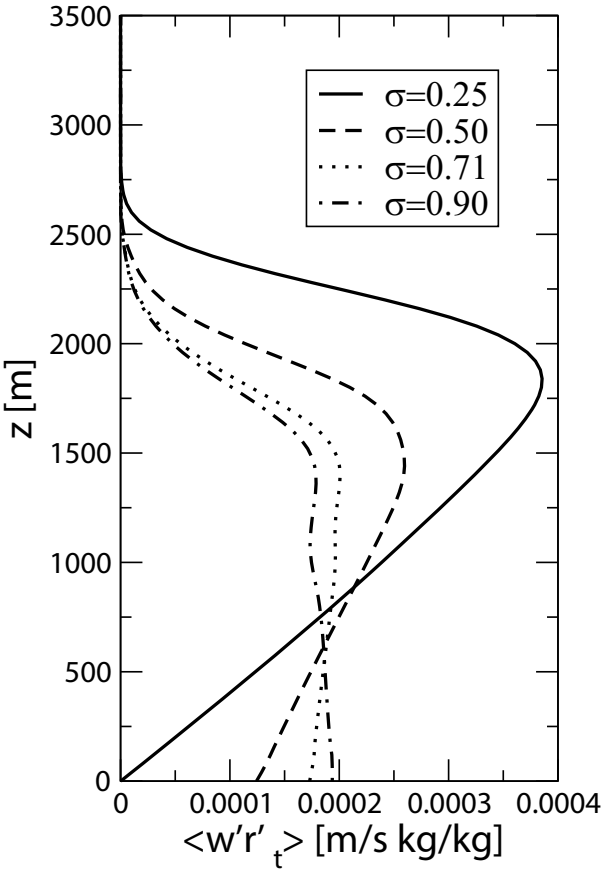

Figure 7: Vertical profiles of total (resolved plus subgrid-scale) turbulent moisture fluxes $\langle w'r'_t \rangle$ for soil saturation ratios σ of 0.25, 0.50, 0.71 and 0.9, respectively (results derived from the reference simulation and simulation set STD). All profiles are 1-h averaged centred at 19:00 UTC. Line patterns as in Figure 6.

To illustrate the effect of different soil moisture contents on cloud characteristics, the temporal development of (a) cloud cover and (b) cloud base height and cloud top height are shown in Fig. 8. Again, we find that after the rapid initial increase in cloud cover which occurs around 15:30 UTC, cloud fractions decrease slowly with time after they reach their maximum value around 18:00 UTC. For the driest soil the maximum cloud cover arrives only at 15 %. The cloud cover increases with increasing soil moisture and peaks at about 30 % for the moistest soil with $\sigma = 0.9$. Moreover, not only the cloud cover, but also the vertical extent of clouds varies as function of soil moisture content (see Fig. 8b). We find that with increasing soil moisture contents (and corresponding larger surface latent heat fluxes) cloud formation starts at lower altitudes. This appears reasonable, because over a wetter soil more water vapour is released into the boundary layer. At the same time, the boundary layer grows less fast as a result of reduced surface sensible heat fluxes. Therefore, more water vapour is distributed over a shallower vertical area resulting in a moister boundary layer in which the cumulus condensation level occurs at heights lower than over drier soils. Finally, we find that cloud formation occurs earlier over drier soils than over wetter soils because of the faster boundary layer growth over drier soils. The strength of the different processes that may influence the formation of boundary layer clouds is quantified by an analysis of the individual contributions to the tendency of the relative humidity at the top of the mean cloud layer and will be discussed in section 4.2.2.

4.2.2 Effect of atmospheric stratification and moisture content

In this section the effect of different initial profiles of liquid water potential temperature and total water mixing ratio on boundary layer and cloud development will be assessed. First, the influence of different thermal stratifications is examined. For this purpose results of simulations in a more stably stratified environment (i.e., set M_STABLE) and runs with a less stable stratification (i.e, set L_STABLE) are compared to those utilizing the standard setup (i.e., set STD). The corresponding initial profiles of liquid water potential temperature are displayed in Fig. 1. Each set consists of sixteen simulations with soil moisture saturation ratios between $\sigma = 0.25$ and $\sigma = 1.0$ (see Table 2).

Fig. 9 compares the profiles of liquid water potential temperature obtained from simulations with different stabilities by showing the corresponding profiles at 18:00 UTC (corresponding to 12:00 local time). For illustration, only results of a wet and a dry soil case are compared with corresponding results using the same soil moisture contents but different thermal stratifications. For the wet case a surface soil moisture saturation ratio of $\sigma = 0.9$ is used, while for the dry case the soil moisture saturation ratio was chosen to be $\sigma = 0.25$. It can be seen that in the more stable case regardless of the soil moisture content a shallower boundary develops compared to the standard case owing to a slower boundary layer growth. In contrast, in the less stably stratified atmosphere the boundary layer is growing much faster compared to the standard case. For dry soil the differences in boundary layer heights amount to about 500 m in the stable case and to about 800 m in the less stable case relative to the run with standard stratification. Due to the smaller increase of potential temperature with height above the boundary layer in the less stably stratified atmosphere, the air that is mixed into the boundary layer is colder than in the standard case. This results in a colder boundary layer. Similarly, the boundary layer is slightly warmer in the case of a more stable stratification, since due to the larger lapse rate above the boundary layer warmer air than in the standard case is entrained into and mixed with the boundary layer air masses. The features described above can also be seen over wet soil. However, over wet soil the differences between the different temperature profiles are not as pronounced as over dry soil, but the tendencies are similar to those observable over dry soil.

With respect to the simulated cloud cover our results are summarized in Fig. 10, where the dependence

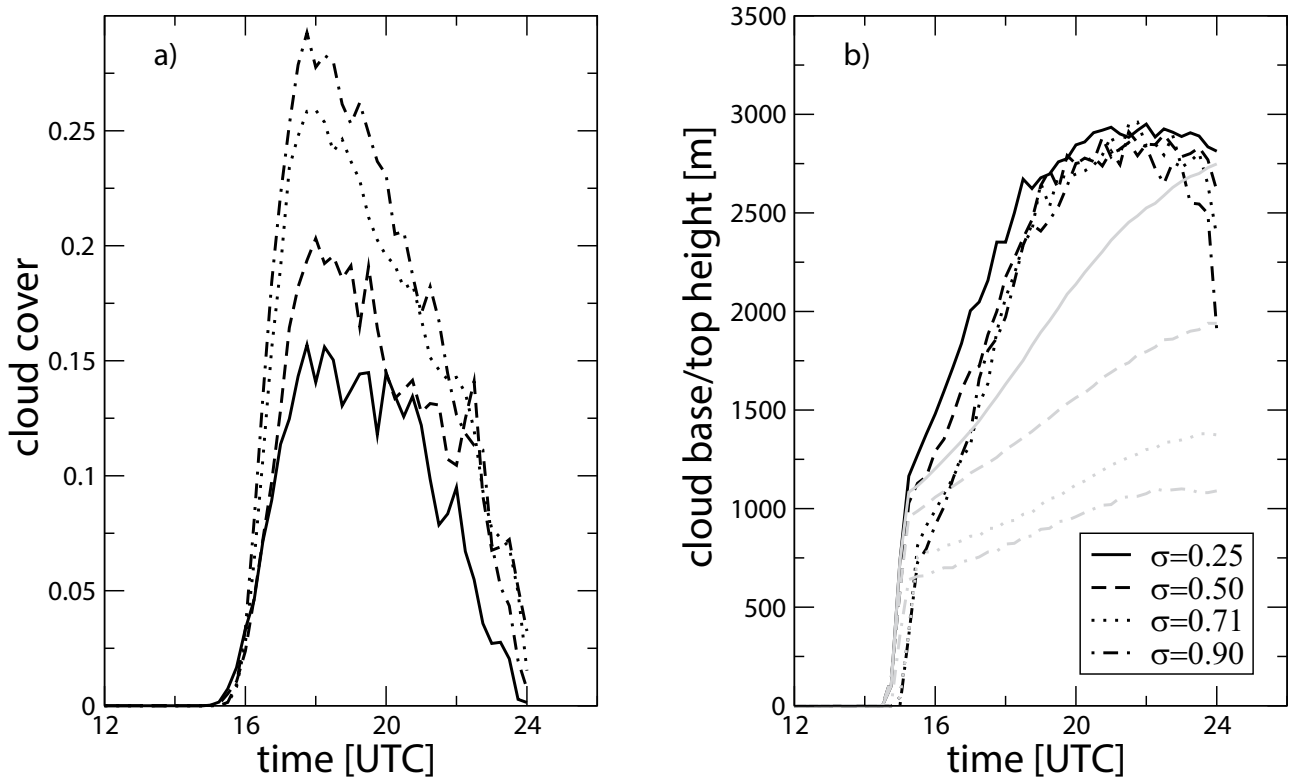

Figure 8: Temporal development of (a) cloud cover, and (b) cloud base height and cloud top height for soil saturation ratios σ of 0.25, 0.50, 0.71, and 0.9, respectively (results derived from the reference simulation and simulation set STD). Line patterns as in Figure 6, cloud top heights in black, cloud base heights in grey.

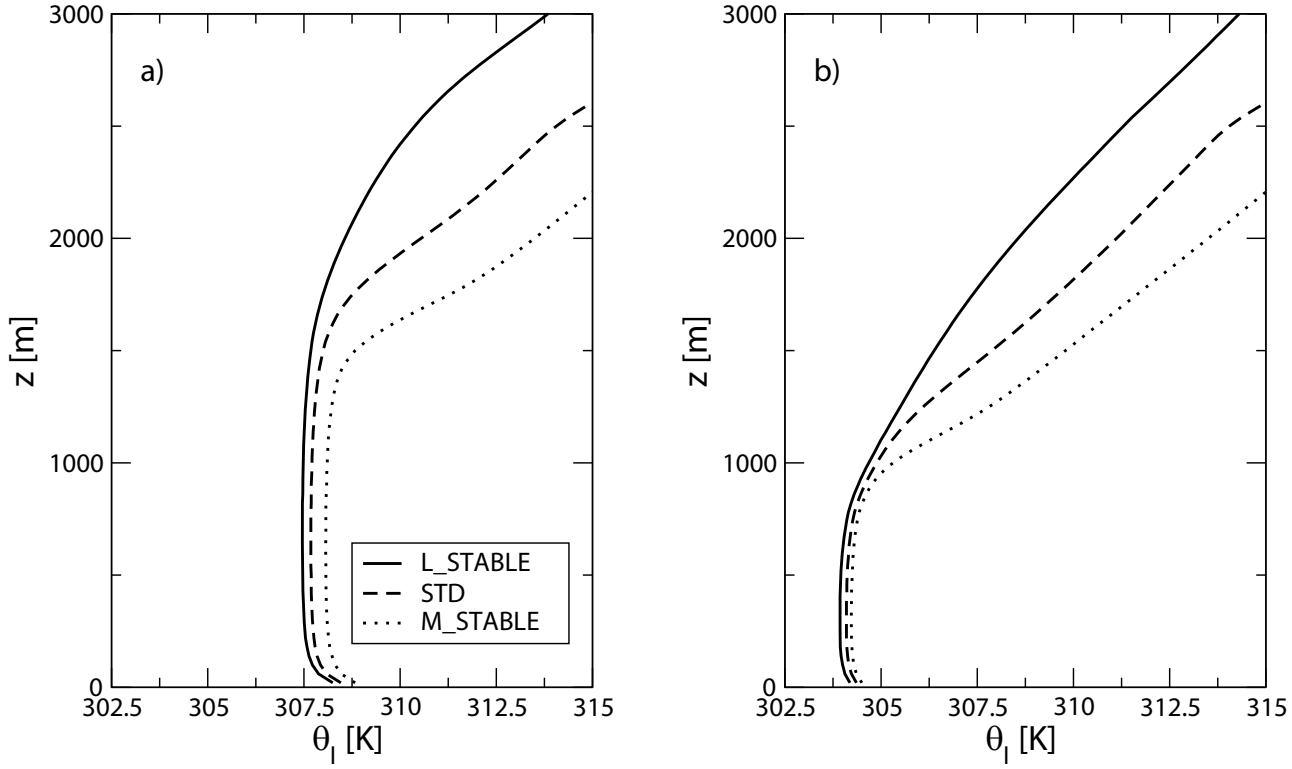

Figure 9: Profiles of liquid water potential temperature for the less stably, the standardly, and the more stably stratified case. Shown are profiles over (a) dry soil with σ = 0.25 in the left panel, and (b) over wet soil with σ = 0.9 in the right panel (results derived from simulation sets STD, L_STABLE, and M_STABLE). All profiles are 1-h averaged centred at 18 UTC.

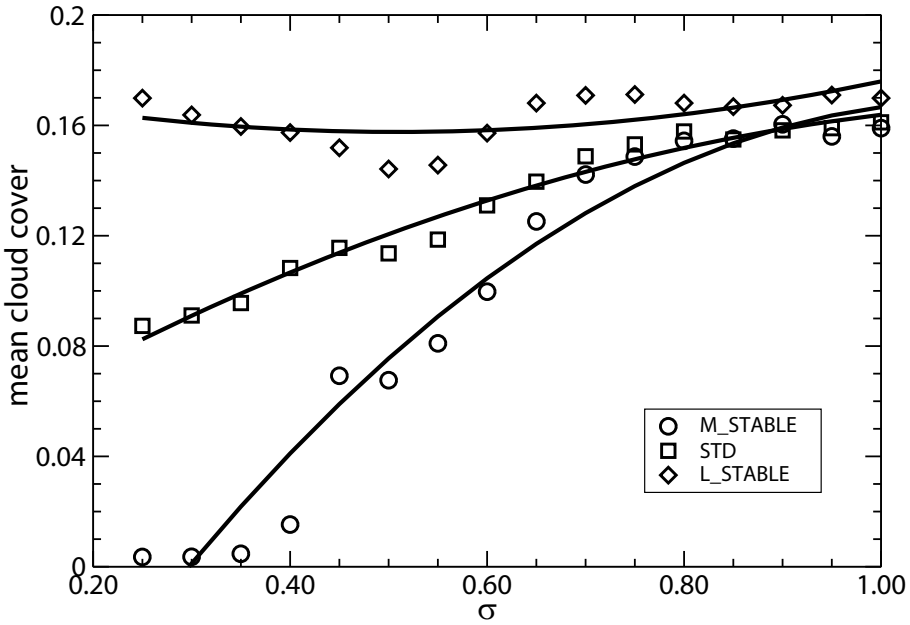

Figure 10: Dependence of the time averaged (averaging interval 15:00 UTC–24:00 UTC) cloud cover on soil moisture content is shown for a more stably (circles), the standardly (squares), and a less stably (diamonds) stratified atmosphere, respectively (results from simulation sets STD, L_STABLE, and M_STABLE). Lines are quadratic fits to guide the eye.

of the time averaged (averaging interval 15:00 UTC–24:00 UTC) cloud cover on soil moisture content is shown for the more stably (circles), the standardly (squares), and a less stably (diamonds) stratified atmosphere, respectively. In the more stably stratified case one can clearly see that for very dry soils cloud development is suppressed and nearly not noticeable. With increasing soil moisture content a broad range exists in which cloud cover is monotonously increasing until the curve saturates. In the standard case, clouds already form over dry soil. Again, the average cloud cover increases monotonously with increasing soil moisture content, and for the wettest soil the average cloud cover is nearly twice as large as over dry soil. In contrast, in case of a less stably stratified atmosphere, the largest time averaged cloud cover (17 %) occurs over the driest soil. This is about two times larger than over the same surface with standard atmospheric stratification. Increasing soil moisture content slightly reduces cloud cover until it reaches a broad minimum with a value of 14 % at a soil moisture saturation ratio of $\sigma = 0.5$. With a further increase of the soil moisture content, the cloud cover increases again. Over the wettest soil the time averaged cloud cover arrives at 17 % which is comparable to the value in the corresponding cases with standard stratification and more stable stratification, respectively. This means that in contrast to the standard case, where cloud cover is a monotonously increasing function of soil moisture, in a less stably stratified atmosphere the averaged cloud cover is a non-monotonous function of soil moisture content and gives values for the time averaged cloud cover that are comparable in magnitude over dry soil and over wet soil. In addition, the variation in cloud cover as a function of stratification is much larger over dry soil than over a wet soil, where the time averaged cloud cover is almost independent of the stratification. The distinct sensitivities are caused by the fact that over dry soil, where the sensible heat flux is large relative to the latent heat flux, the boundary layer growth which controls cloud development is strongly affected by the thermal stratification of the atmosphere. Water vapour is mixed upward by daytime turbulence and thermal driven convection that form clouds at the top of the rapidly growing boundary layer. In contrast, over wet soil with small sensible heat fluxes cloud development is mainly dependent on the magnitude of the latent heat flux at the surface and is not very much influenced by the stability of the overlying atmosphere. Similar conclusions have been drawn by Ek and Mahrt (1994) and Ek and Holtslag (2004) using a simpler modelling approach.

In the following, to understand the complex interplay of the different processes that may promote or suppress the formation of shallow boundary layer clouds, we will analyse and interpret our LES results by applying the relative humidity tendency equation at the top of the mean cloud layer (which is defined here as the mean cloud top height h_{MCT}), i.e. the average height at which cloud tops occur. This technique has proven to be a valuable diagnostic tool, because the relative humidity is a key variable controlling cloud formation and development in the boundary layer. Many physical processes that govern the interaction and feedbacks between the land surface and the overlying atmosphere are involved in this equation and determine its temporal evolution (e.g., Ek and Mahrt, 1994; Ek and Holtslag, 2004; van Heerwaarden et al., 2010; Huang and Margulis, 2011). Using the definition for the rel-

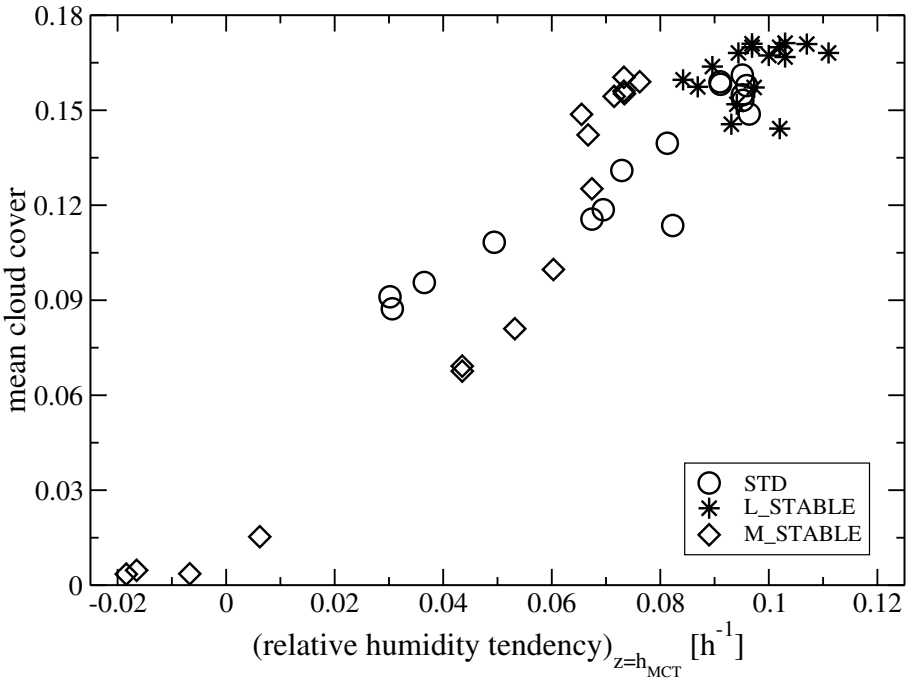

Figure 11: Scatter plot of time averaged cloud cover and mean relative humidity tendency at the top of the mean cloud layer (mean cloud top height h_{MCT}) for all runs (utilizing the standard initial total water mixing ratio profile) as simulated with the coupled LES-LSM model (simulation sets STD, L_STABLE, and M_STABLE).

ative humidity $RH = r_{\mathrm{v}}/r_{\mathrm{v,s}}$, the tendency equation for the relative humidity at the top of the mean cloud layer can be written (see e.g., Ek and Mahrt, 1994) as follows:

$$\left(\frac{1}{RH}\frac{\partial RH}{\partial t}\right)_{z=h_{\mathrm{MCT}}} = \left(\frac{1}{r_{\mathrm{v}}}\frac{\partial r_{\mathrm{v}}}{\partial t}\right)_{z=h_{\mathrm{MCT}}} - \left(\frac{1}{r_{\mathrm{v,s}}}\frac{dr_{\mathrm{v,s}}}{dT}\right)_{z=h_{\mathrm{MCT}}} \left(e^{-\frac{R}{c_p}\frac{h_{\mathrm{MCT}}}{H_{\mathrm{s}}}}\left(\frac{\partial \theta}{\partial t}\right)_{z=h_{\mathrm{MCT}}} - \frac{g}{c_p}\frac{\partial h_{\mathrm{MCT}}}{\partial t}\right), \tag{4.1}$$

where r_{v} denotes the water vapour mixing ratio, $r_{\mathrm{v,s}}$ is the saturation water vapour mixing ratio, $dr_{\mathrm{v,s}}/dT$ is the slope of the saturation mixing ratio-temperature curve, T is temperature, θ is potential temperature, H_{s} is the scale height of the atmosphere, R is the individual gas constant for dry air, c_p is the specific heat at constant pressure, and h_{MCT} is the mean cloud top height. The three terms on the right hand side of Eq. (4.1) denote the following relative humidity tendencies as the result of

- boundary layer moistening/drying due to a latent surface heat flux and/or an entrainment flux that transports drier air from the free atmosphere into the boundary layer;
- boundary layer warming due to sensible surface heat flux and entrainment of warmer air at the top of the boundary layer;
- an increase of boundary layer depth that results in an increase of relative humidity as for a given potential temperature the actual temperature in the cloud layer will decrease with boundary layer growth.

The relevance of these different processes for the cloud development in different atmospheric and soil conditions will now be evaluated using data from our LES runs. Here, we calculated the different terms in Eq. (4.1), and they were additionally averaged over time; time averages are taken over the period 15:00–19:00 UTC for the less stable cases and 16:00–20:00 UTC for the standard and the more stable cases. First, Fig. 11 demonstrates that the relative humidity tendency concept is a useful idea to predict cloud development, because it shows a clear (linear) relationship between mean cloud cover and the relative humidity tendency. In Fig. 12 the various terms that contribute to the relative humidity tendency are plotted as a function of the soil moisture content separately for the different thermal stabilities. For all stability classes the boundary layer warming term tends to reduce the relative humidity in the boundary layer as a result of a surface heat flux and an entrainment heat flux at the top of the boundary layer. The reduction in relative humidity is of the same magnitude for all stabilities and decreases with increasing soil moisture content. Similarly, the boundary layer moistening term is always negative for less stable conditions, because the entrainment drying is larger than the moistening of the boundary layer due to a positive surface moisture flux. For the standard case and especially in the more stable case, the boundary layer moistening term changes sign and becomes positive with increasing soil moisture contents, because due to the slower boundary layer growth less dry air is entrained into the boundary layer. The boundary layer cooling term due to the boundary layer growth which tends to increase the rela-

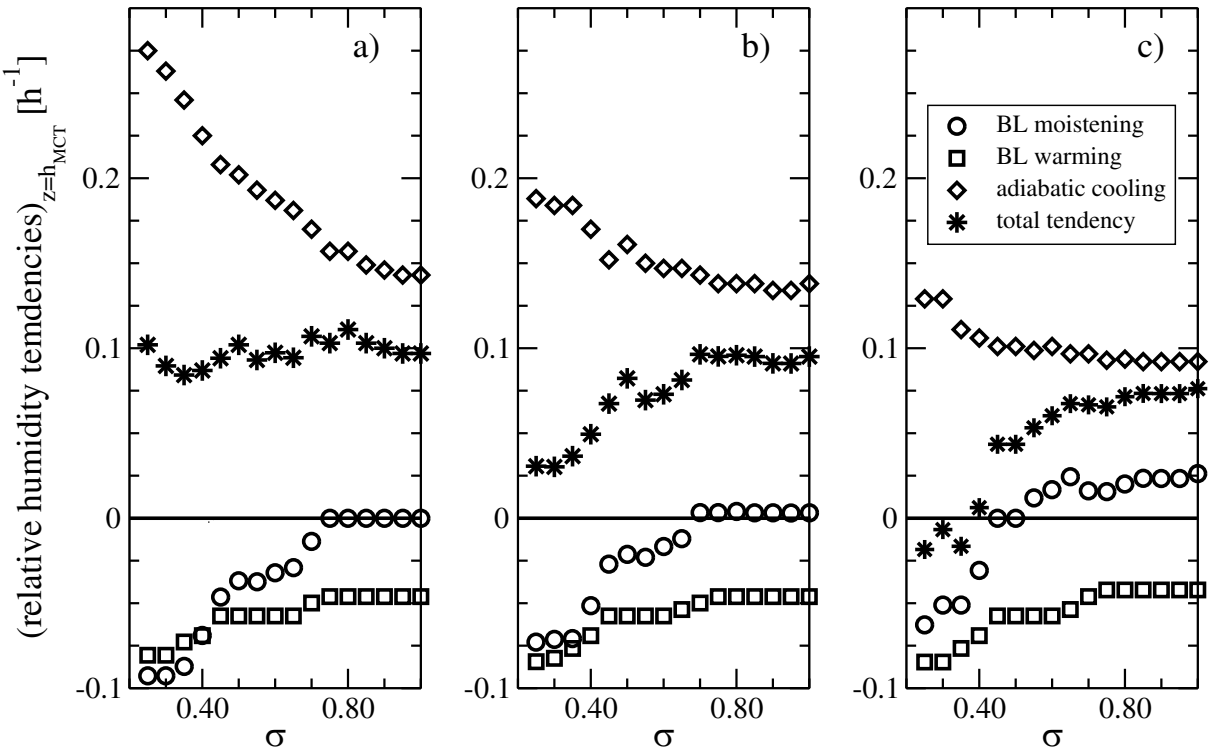

Figure 12: Various terms that contribute to the relative humidity tendency at the top of the mean cloud layer (mean cloud top height h_{MCT} are plotted as function of the soil moisture content for (a) less stable conditions, (b) the standard case, and (c) the more stable case derived from simulations with the coupled LES-LSM model (simulation sets STD, L_STABLE, and M_STABLE). Shown are tendencies of relative humidity due boundary layer moistening (circles), boundary layer warming (squares), adiabatic cooling (diamonds), and the total tendency (stars), respectively.

tive humidity is the dominant term in the relative humidity tendency equation for all stability classes. However, in the case of more stable conditions and in the standard case the sum of boundary layer warming and boundary layer drying more than compensates the adiabatic cooling over dry soil resulting in small relative humidity tendencies. These total tendencies otherwise increase with increasing soil moisture content and are largest over the wettest soil. In contrast, for less stable conditions the boundary layer growth over dry soil is much faster than in the standard and the more stable cases, because less work has to be done against the buoyancy forces. As a result, the boundary layer cooling term balances out or even overcompensates the boundary layer warming and drying terms producing a flat total relative humidity tendency curve that varies weakly with increasing soil moisture content.

In the following, the influence of the atmospheric moisture content on the boundary layer development is examined. Here, we explore the sensitivity of the model results with respect to a shift of the initial total water mixing ratio profile. This investigation is motivated by an understanding that besides the thermal stratification the atmospheric moisture content is the most important thermodynamic variable that determines the boundary layer and cloud development. First, we performed additional runs, where the initial total water vapour mixing ratio has been increased (decreased) by $1\,\mathrm{g\,kg^{-1}}$ at every grid point (see Fig. 1 that displays the different initial profiles). Simulations have been performed for the whole spectrum of soil moisture contents and thermal stratifications (simulation sets STD, STD_DRY, STD_MOIST, L_STABLE, L_STABLE_DRY, L_STABLE_MOIST, M_STABLE, M_STABLE_DRY, and M_STABLE_MOIST, see also Table 2). The results of these runs are shown in Fig. 13, where the mean cloud cover is plotted against soil moisture content. Obviously, in a slightly dryer atmosphere no clouds develop over dry soil in the standard and the more stable case. However, if the soil moisture saturation ratio σ exceeds 0.4, the mean cloud cover monotonously increases with soil moisture content until a saturation value is attained in the limiting case of a water saturated soil. In the less stable case, the coupling between the soil moisture and cloud cover is weak, as the mean cloud cover is almost independent of σ. In a moister atmosphere cloud development is possible even over dry soil. Again, mean cloud cover increases with increasing soil moisture content for the more stable and the case with standard stratification. In case of less stable stratification, mean cloud cover is largest over dry soil and decreases with increasing soil moisture content. Finally, we would like to point out that in the limiting case of a water saturated soil, the mean cloud cover appears to be almost independent of the stratification and depends only on the atmospheric moisture content. In the dry at-

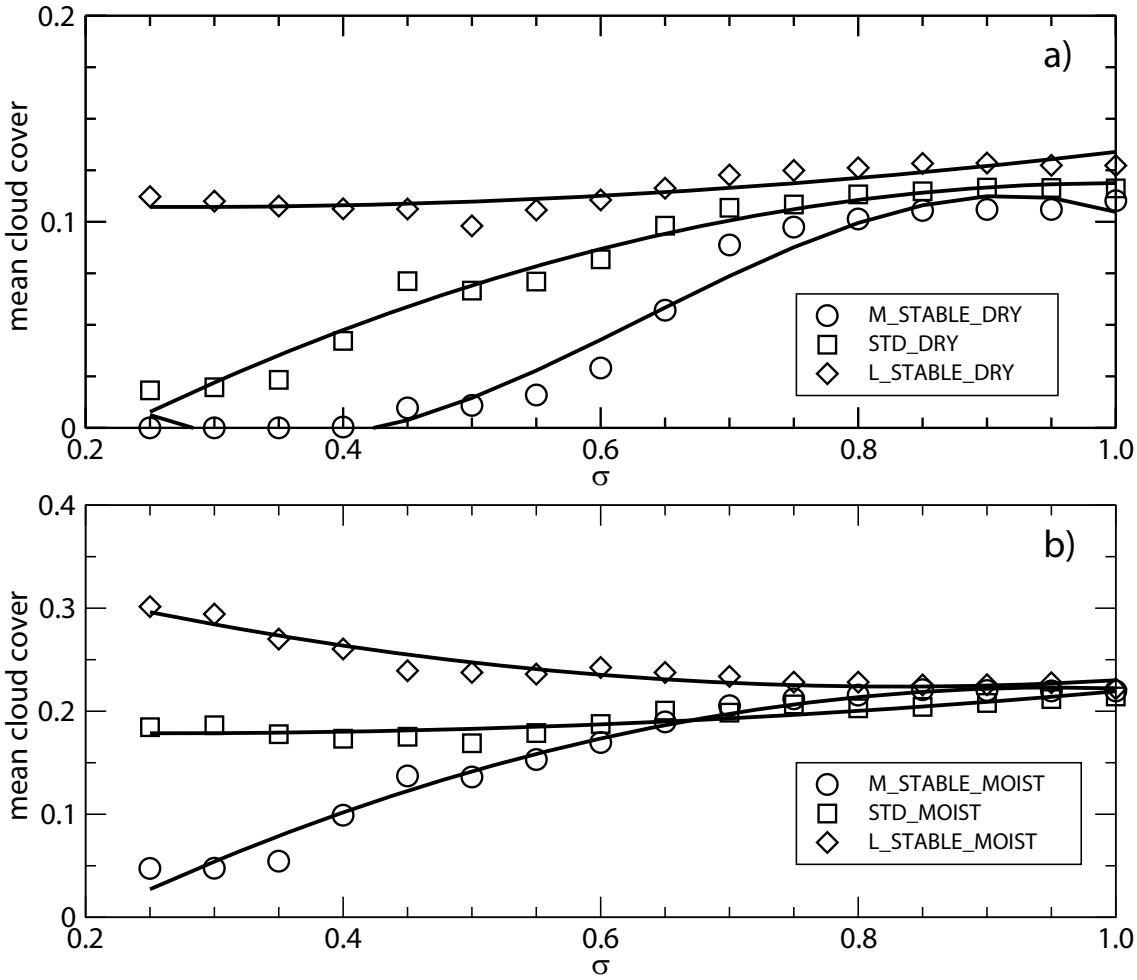

Figure 13: Time averaged (averaging interval 15:00 UTC–24:00 UTC) cloud cover versus soil moisture content for a more stably (circles), the standardly (squares), and a less stably (diamonds) stratified atmosphere, respectively, as simulated with the coupled LES-LSM model in (a) a dry atmosphere, in which the initial total water mixing ratio profile has been shifted by −1 g/kg relative to the standard profile (results derived from sets STD_DRY, L_STABLE_DRY, and M_STABLE_DRY), and (b) in a moist atmosphere in which the initial total water mixing ratio profile has been shifted by +1 g/kg relative to the standard profile (results derived from sets STD_MOIST, L_STABLE_MOIST, and M_STABLE_MOIST). Lines are quadratic fits to guide the eye.

mospheric case, the mean cloud cover amounts to 12 %, in an atmosphere with the standard moisture profile a value of 17 % is attained, and in the moist atmospheric case, an average cloud cover of 22 % is attained in the limiting case of a water saturated soil. We have to admit that the limited sensitivity of mean cloud cover to variations of atmospheric stability in the limit of a water saturated soil is a feature that we have not fully understood. This behaviour can probably partly explained by the fact that the boundary layer growth rate over wet soil is greatly reduced for all stabilities. Moreover, this feature is consistent with the results of our relative humidity tendency analysis which reveal that the interplay of the different processes results into a total relative humidity tendency that is insensitive to variations of static stability but depends on soil and atmospheric moisture content.

Second, a similar analysis as above has been performed for cases in which the initial moisture profile has been modified only between 1300 m and 2500 m and in the free atmosphere, where the initial mean total water mixing ratio is assumed to be constant with height. The initial total water mixing ratio profile has been varied for heights above 2500 m in steps of $2\,\mathrm{g\,kg^{-1}}$ beginning with an initial total water mixing ratio of $r_{\mathrm{t,top}} = 1\,\mathrm{g\,kg^{-1}}$ and ending with $r_{\mathrm{t,top}} = 5.0\,\mathrm{g\,kg^{-1}}$. Linear interpolation was used to obtain values at intermediate levels between 1300 m–2500 m (see Fig. 1). Simulations have been performed for all stratifications and the full spectrum of soil moisture contents (simulation sets STD, STD_DRY_FA, STD_MOIST_FA, L_STABLE, L_STABLE_DRY_FA, L_STABLE_MOIST_FA, M_STABLE, M_STABLE_DRY_FA, and M_STABLE_MOIST_FA, see also Table 2). In Fig. 14 we see that in the cases of more stable and standard stratifications mean cloud cover is only slightly affected by moisture content in the free atmosphere. This is understandable, because boundary layer growth is rather slow even over dry soil in these cases.

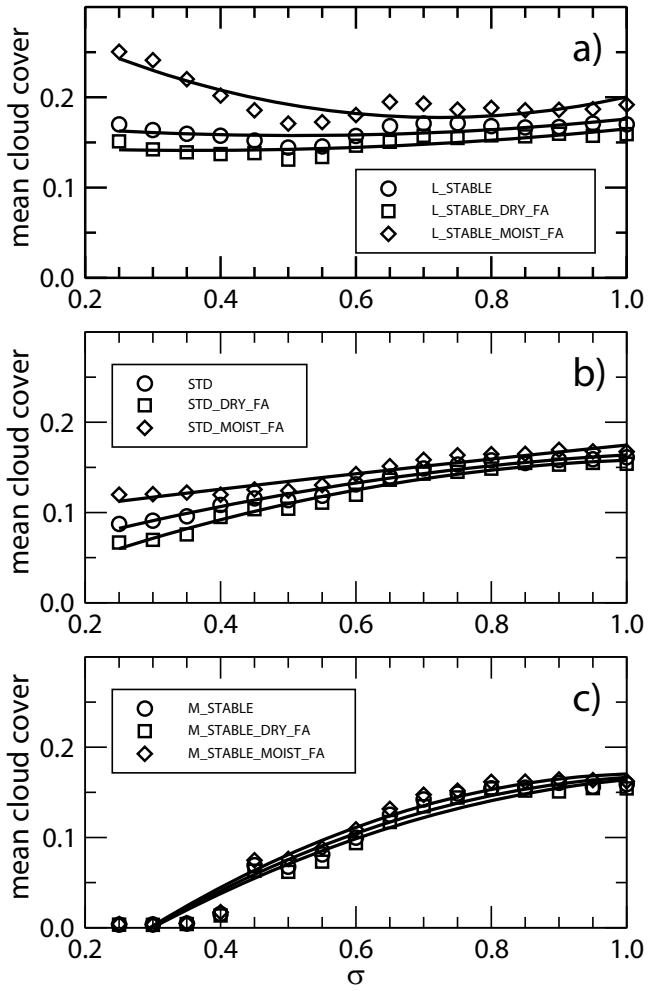

Figure 14: Time averaged (averaging interval 15:00 UTC–24:00 UTC) cloud cover versus soil moisture content for (a) less stable stratification (results derived from sets L_STABLE, L_STABLE_MOIST_FA, L_STABLE_DRY_FA), (b) standard stratification (results derived from sets STD, STD_MOIST_FA, STD_DRY_FA), and (c) more stably stratified atmosphere (results derived from sets M_STABLE, M_STABLE_MOIST_FA, M_STABLE_DRY_FA). Here, the initial total water mixing ratio profiles have been modified in the interval 1300 m–2500 m and in the free atmosphere, where the initial mean total water mixing ratio is assumed to be constant with height. Lines are quadratic fits to guide the eye.

As a consequence, the developing boundary layer is too shallow to be influenced by air parcels that originate from heights above 2000 m. In contrast, for a less stably stratified atmosphere a significant impact of the free tropospheric moisture content especially over dry soil on the boundary layer cloudiness is observable. In this case, the boundary layer appears deep enough so that entrainment of free tropospheric air influences the cloud development within the boundary layer. In case of a dry free atmosphere with a water vapour mixing ratio of $r_{\mathrm{t,top}} = 1\,\mathrm{g\,kg^{-1}}$, the (positive), entrainment flux of moisture increases at the top of the boundary layer i.e., more dry air is engulfed into the boundary layer tending to reduce the mean water vapour mixing ratio, which tends to reduce the mean cloud cover. Conversely, for $r_{\mathrm{t,top}} = 5\,\mathrm{g\,kg^{-1}}$ the entrainment flux of moisture is strongly reduced owing to the smaller difference in total water mixing ratio between the free troposphere and the top of boundary layer. This results in a smaller boundary layer drying. As a consequence, mean cloud cover increases compared to the standard case with $r_{\mathrm{t,top}} = 3\,\mathrm{g\,kg^{-1}}$. The largest difference in mean cloud cover between the $r_{\mathrm{t,top}} = 5\,\mathrm{g\,kg^{-1}}$ and $r_{\mathrm{t,top}} = 3\,\mathrm{g\,kg^{-1}}$ occurs over the driest soil, because the reduction in the entrainment flux of moisture is largest here owing to the most rapid boundary layer growth. These results clearly demonstrate that not only the water vapour content within the boundary layer influences cloud development, but that especially in a less stably stratified atmosphere mean cloud cover depends quite sensitively on the water vapour content above the boundary layer. Our results are supported by the findings of Vilà-Guerau de Arellano (2007) who analysed thermodynamic profiles taken by radiosondes at the SGP ARM site at two consecutive nights. He investigated the role of the nocturnal boundary layer and its layer above in setting up appropriate conditions for triggering shallow cumulus convection. According to this study the most important observed conditions favourable for cloud formation are a reduction in the potential temperature and moisture jump at the boundary layer-free atmosphere interface.

We also performed a relative humidity tendency analysis for the runs using different initial atmospheric humidity profiles. We did not display results of this analysis because these are structurally quite similar to those obtained with the standard atmospheric humidity profile. In the simulations that utilize the shifted humidity profiles the contributions of the different processes to the relative humidity tendency remain almost unchanged with the exception of the term that results from the cloud layer growth. In the moist (dry) case a larger (smaller) adiabatic cooling at the top of the mean cloud layer occurs. This occurs because in the moist (dry) case a deeper (shallower) cloud layer develops that produces more (less) vigorous cloud circulations reaching higher (lower) mean cloud top heights characterized by colder (warmer) absolute temperatures relative to the simulation that uses the standard atmospheric humidity profile. In those simulations in which only the upper tropospheric moisture content has been increased (decreased) the potential for shallow cumulus cloud development is enhanced (reduced) due to a larger (smaller) net relative humidity tendency. In these cases, the tendencies due to boundary layer warming and the growth of the cloud layer height are almost unchanged relative to the runs that use the standard initial atmospheric humidity profile. However, the tendency contribution that governs the decrease in relative humidity due to boundary layer drying is reduced (less negative) in an atmosphere with a moister free troposphere (simulation set MOIST_FA) and is enhanced (more negative) in an atmosphere with a dryer free troposphere (simulation set DRY_FREE_FA),

respectively. This is reasonable because the drying of the cloud layer by entrainment is proportional to the difference in water vapour mixing ratio at the top of the cloud layer.

5 Summary and conclusions

In this paper the effect of soil moisture and atmospheric conditions on the diurnal development of shallow cumulus convection over land is investigated using a coupled LES-LSM. Several simulations have been performed with different amounts of soil moisture content and varying profiles of both, liquid water potential temperature and total water mixing ratio in the ABL and in the free atmosphere.

First, we demonstrated, using an idealisation of an observed case of shallow cumulus clouds at the SGP site of the ARM Program on 21 June 1997, that the coupled model is in principle suitable to reproduce the mean features of the diurnal cycle of shallow cumulus convection. Furthermore, simulated characteristics of the developing cloud topped boundary layer are consistent with results obtained in the context of the sixth intercomparison of GCSS Working Group 1 modelling exercise that addressed the same case (see Brown et al., 2002).

Second, an extensive sensitivity study has been performed in which different initial values of the soil moisture content have been applied, but where the initial atmospheric state remained unchanged. Our results confirm the hypothesis of Ek and Mahrt (1994) and Ek and Holtslag (2004), and corroborate the results of Huang and Margulis (2011), that the static stability of the atmosphere influences the response of shallow cumulus convection to variations in soil moisture content. In the simulations utilizing the standard temperature profile or a more stably stratified boundary layer, cloud cover is larger over wet soils than over dry soils. An analysis of the relative humidity tendency equation reveals that as a result of the large latent heat flux at the surface, the largest growth of relative humidity occurs over wet soils, which tends to promote the development of clouds. In contrast, over dry soils the turbulent surface moisture fluxes are smaller and the entrainment of moisture at the top of the boundary layer is larger compared to the wet soil case which prevent, together with the slow boundary layer growth due to the more stably stratified atmospheric environment, a sufficient moistening at the top of the boundary layer. Therefore, the relative humidity tendency is smaller over dry soils than over wet soils resulting in a positive soil moisture-cloud cover coupling. In the case of a less stably stratified boundary layer, the soil moisture cloud coupling is rather weak, as cloud cover appears almost independent to variations in soil moisture. Over dry soil vigorous convection develops leading to fast boundary layer growth producing a strong adiabatic cooling at the top of the boundary layer. However, boundary layer warming due to surface heating and entrainment warming as well as boundary layer drying partially compensate the tendency in relative humidity due to adiabatic cooling. Over wet soil the adiabatic cooling tendency is greatly reduced, but in the same proportion also the two compensating processes diminish, thereby producing a relative humidity tendency curve that is flat relative to variations in soil moisture content.

Moreover, we note that the variation of cloud cover due to a change of soil moisture is not only influenced by the thermal stability but is also strongly dependent on the atmospheric moisture content. In a dry (moist) atmosphere mean cloud cover is always smaller (larger) than in the run using the standard moisture profile (when comparing among cases with the same thermal stability). Remarkably, in a less stably stratified moist atmosphere the largest mean cloud cover occurs over dry soil and decreases with increasing soil moisture content. This implies that in a moist atmosphere the total relative humidity tendency, which is largest in this case over dry soil, is dominated by the adiabatic cooling term. Another important result is that in the limiting case of a water saturated soil (i.e., in the case that the soil moisture saturation ratio approaches one) the simulated mean cloud cover is independent of the thermal stratification, but depends only on the integrated water vapour content in a vertical column. The simulations in which only the water vapour mixing ratio in the free atmosphere has been modified, the most noticeable variations of the cloud amount occur over dry soil in a less stable environment. In this case, the maximum mean cloud cover again occurs over the driest soil, since the boundary layer growth is fast enough so that the moisture entrainment flux is influenced by the air in the free troposphere. In case of a moister free atmosphere the entrainment flux of moisture is heavily reduced (less mixing of dry air into the boundary layer) leading to a smaller boundary layer drying which in turn results in more clouds.

We conclude that soil moisture, atmospheric static stability, and water vapour content should play an important and equal role in future modelling and parameterization efforts of boundary layer clouds over land because of their prominent influence on the atmospheric moisture budget and on the fractional cloud cover. We hope that those who try to advance the parameterization of cloud related processes in general circulation and numerical weather prediction models may benefit from our sensitivity study. Since the LES approach is more fundamental to the simulation of boundary layer cloud processes, as it explicitly resolves most of the energetic eddies that do most of the transports, it offers a semi-empirical basis for parameterization improvement and development. Results of our sensitivity study may be used to produce a comprehensive data set on the diurnal cycle of shallow cumulus clouds that can be used to evaluate parameterizations and to identify deficiencies in these representations of boundary layer processes.

Acknowledgements

The study was supported by the Max Planck Society for the advancement of science. Use of the supercomputer facilities at the Deutsches Klimarechenzentrum

(DKRZ) is acknowledged. The authors would like to thank Kirsten Warrach for providing the source code of the land surface model SEWAB.

References

Betts, A.K., M.A.F. Silva Dias, 2010: Progress in understanding land-surface-atmosphere coupling over the Amazon: a review. – J. Adv. Model. Earth Syst. **2**, published online, DOI:10.3894/JAMES.2010.2.6.

Betts, A.K., J.H. Ball, A.C.M. Beljaars, M.J. Miller, P.A. Viterbo, 1996: The land surface-atmosphere interaction: A review based on observational and global modelling perspectives. – J. Geophys. Res. **101**, 7209–7225.

Best, M.J., A. Beljaars, J. Polcher, P. Viterbo, 2004: A proposed structure for coupling tiled surfaces with the planetary boundary layer. – J. Hydrometeorol. **5**, 1271–1278.

Brown, A.R., R.T. Cederwall, A. Chlond, P.K. Duynkerke, J.-C. Golaz, M. Khairoutdinov, D.C. Lewellen, A.P. Lock, M.K. MacVean, C.-H. Moeng, R.A.J. Neggers, A.P. Siebesma, B. Stevens, 2002: Large-eddy simulation of the diurnal cycle of shallow cumulus convection over land. – Quart. J. Roy. Meteor. Soc. **128**, 1075–1093.

Chlond, A., 1992: Three-dimensional simulation of cloud street development during a cold air outbreak. – Bound.-Layer Meteor. **58**, 161–200.

Chlond, A., 1994: Locally modified version of Bott's advection scheme. – Mon. Wea. Rev. **122**, 111–125.

Cook, B.I., G.B. Bonan, S. Levis, 2006: Soil moisture feedbacks to precipitation in southern Africa. – J. Climate **19**, 4198–4206.

Deardorff, J. W., 1978: Efficient prediction of ground surface temperature and moisture with inclusion of a layer of vegetation. – J. Geophys. Res. **83**, 1889–1903.

Deardorff, W., 1980: Stratocumulus-capped mixed layers derived from a three-dimensional model. – Bound.-Layer Meteor. **18**, 495–527.

Derbyshire, S., I. Beau, P. Bechthold, J.-Y. Grandpeix, J.-M. Piriou, J.-L. Redelsperger, P.M.M. Soares, 2004: Sensitivity of moist convection to environmental humidity. – Quart. J. Roy. Meteor. Soc. **130**, 3055–3079.

Duchon, C.E., K.G. Hamm, 2005: Broadband albedo observations in the Southern Great Plains. – J. Appl. Met. Climatol. **45**, 210–234.

Ek, M., L. Mahrt, 1994: Daytime evolution of relative humidity at the boundary layer top. – Mon. Wea. Rev. **122**, 2709–2721.

Ek, M., A.A.M. Holtslag, 2004: Influence of Soil Moisture on Boundary Layer Cloud Development. – J. Hydrometeorol. **5**, 86–98.

Findell, K.L., E.A.B. Eltahir, 1997: An analysis of the soil moisture-rainfall feedback, based on direct observations from Illinois. – Water Resour. Res. **33**, 725–735.

Findell, K.L., E.A.B. Eltahir, 2003a: Atmospheric controls on soil moisture-boundary layer interactions. Part I: Framework development. – J. Hydrometeorol. **4**, 552–569.

Findell, K.L., E.A.B. Eltahir, 2003b: Atmospheric controls on soil moisture-boundary layer interactions. Part II: Feedbacks within the continental United States. – J. Hydrometeorol. **4**, 570–583.

Findell, K.L., P. Gentine, B.R. Lintner, C. Kerr, 2011: Probability of afternoon precipitation in eastern United States and Mexico enhanced by high evaporation. – Nature Geoscience **4**, 434–439. DOI:10.1038/NGEO1174.

Gentine, P., C.R. Ferguson, A.A.M. Holtslag, 2013: Diagnosing evaporative fraction over land from boundary-layer clouds. – J. Geophys. Res. Atmos. **118**, 8185–8196.

Golaz, J.-C., H. Jiang, W.R. Cotton, 2001: A large-eddy simulation study of cumulus clouds over land and sensitivity to soil moisture. – Atmos. Res. **59**, 373–392.

Grant, A.L.M., 1986: Observations of boundary-layer structure made during the KONTUR experiment. – Quart. J. Roy. Meteor. Soc. **112**, 825–841.

Hohenegger, C., P. Brockhaus, C.S. Bretherton, C. Schär, 2009: The soil moisture-precipitation feedback in simulations with explicit and parameterized convection. – J. Climate **22**, 5003–5020.

Huang, H.-Y., S.A. Margulis, 2011: Investigating the impact of soil moisture and atmospheric stability on cloud development and distribution using a coupled large-eddy simulation and land surface model. – J. Hydrometeorol. **12**, 787–804.

Jacobs, C.M.J., H.A.R. De Bruin, 1992: The sensitivity of regional transpiration to land-surface characteristics: Significance of feedback – J. Climate **5**, 683–698.

Koster, R.D., M.J. Suarez, R.W. Higgins, H.M. van den Dool, 2003: Observational evidence that soil moisture variations affect precipitation. – Geophys. Res. Lett. **30**, 1241, DOI:10.1029/2002GL016571, 5.

Koster, R.D., P.A. Dirmeyer, Z. Guo, G. Bonan, E. Chan, P. Cox, C.T. Gordon, S. Kanae, E. Kowalczyk, D. Lawrence, P. Liu, C.-H. Lu, S. Malyshev, B. McAvaney, K. Mitchell, D. Mocko, T. Oki, K. Oleson, A. Pitman, Y.C. Sud, C.M. Taylor, D. Verseghy, R. Vasic, Y. Xue, T. Yamada, 2004: Regions of strong coupling between soil moisture and precipitation. –Science **305**, 1138–1140.

Le Mone, M.A., R.L. Grossman, R.L. Coulter, M.L. Wesley, G.E. Klazura, G.S. Pulos, W. Blumen, J.K. Lundquist, R.H. Cuenca, S.F. Kelly, E.A. Brandes, S.P. Oncley, R.T. McMillen, B.B. Hicks, 2000: Land-atmosphere interaction research, early results, and opportunities in the Walnut River watershed in southeast Kansas: CASES and ABLE. – Bull. Amer. Meteor. Soc. **81**, 757–779.

Lenschow, D.H., J.C. Wyngaard, W.T. Pennel, 1980: Mean-field and second moment budgets in a baroclinic, convective boundary layer. – J. Atmos. Sci. **37**, 1313–1326.

Lohou, F. and E.G. Patton, 2014: Surface energy balance and buoyancy response to shallow cumulus shading. – J. Atmos. Sci. **71**, 665–682, DOI:10.1175/JAS-D-13-0145.1.

Mengelkamp, H.-T., K. Warrach, E. Raschke, 1997: A land surface scheme for atmospheric and hydrologic models: SEWAB (Surface Energy and Water Balance). – Externer Bericht des GKSS Forschungszentrums, GKSS 97/E/69.

Mengelkamp, H.-T., K. Warrach, E. Raschke, 1999: SEWAB – a parameterization of the surface energy and water balance for atmospheric and hydrologic models. – Adv. Water. Res. **23**, 165–175.

Mengelkamp, H.-T., G. Kiely, K. Warrach, 2001: Evaluation of the hydrological components added to an atmospheric land-surface scheme. – Theor. Appl. Climatol. **69**, 199–212.

Neggers, R.A.J., P.G. Duynkerke, S.M.A. Rodts, 2002: Shallow cumulus convection: A validation of large-eddy simulation against aircraft and landsat observations. – Quart. J. Roy. Meteor. Soc. **129**, 2671–2696.

Nicholls, S., M.A. Le Mone, 1980: The fair weather boundary layer in GATE: The relationship of subcloud fluxes and structure to the distribution and enhancement of cumulus clouds. – J. Atmos. Sci. **37**, 2051–2067.

Nicholls, S., C.J. Readings, 1979: Aircraft observations of the lower boundary layer over sea. –Quart. J. Roy. Meteor. Soc. **105**, 785–802.

Pan, Z., E. Takle, M. Segal, R. Turner, 1996: Influences of model parameterization schemes on the response of rainfall to soil moisture in the central United States. – Mon. Wea. Rev. **124**, 1786–1802.

Pielke, R.A., 2001: Influence of the spatial distribution of vegetation and soils on the prediction of cumulus convective rainfall. – Rev. Geophys. **39**, 151–177.

Santanello, J.A., M.A. Friedl, W.P. Kustas, 2005: An empirical investigation of convective planetary boundary layer evolution and its relationship with the land surface. – J. Appl. Meteorol. **44**, 917–932.

Santanello, J.A., M.A. Friedl, M.B. Ek, 2007: Convective boundary layer interactions with the land surface at diurnal time scales: diagnostics and feedbacks. – J. Hydrometeor. **8**, 1082–1097.

Santanello, J.A., C.D. Peters-Lidard, S.V. Kumar, C. Alonge, W.K. Tao, 2009: A modelling and observational framework for diagnosing local and land-atmosphere coupling on diurnal time scales. – J. Hydrometeor **10**, 577–599.

Schlemmer, L., C. Hohenegger, J. Schmidli, C.S. Bretherton, C. Schär, 2011: An idealized cloud-resolving framework for the study of midlatitude diurnal convection over land. – J. Atmos. Sci. **68**, 1041–1057.

Schumann, U., A. Dörnbrack, B. Mayer, 2002: Cloud-shadow effects on the structure of the convective boundary layer. – Meteorol. Z. **11**, 285–294, DOI: 10.1127/0941-2948/2002/0011-0285.

Segal, M., R.W. Arritt, C. Clark, 1995: Scaling evaluation of the effect of surface characteristics on potential for deep convection over uniform terrain. – Mon. Wea. Rev. **123**, 383–400.

Seneviratne, S.I., T. Corti, E.L. Davin, M. Hirschi, E.B. Jaeger, I. Lehner, B. Orlowsky, A.J. Teuling, 2010: Investigating soil moisture-climate interactions in a changing climate: A review. – Earth-Sci. Rev. **99**, 125–161.

Siebesma, A.P., C.S. Bretherton, A. Brown, A. Chlond, J. Cuxart, P.G. Duynkerke, H. Jiang, M. Khairoutdinov, D. Lewellen, C.-H. Moeng, E. Sanchez, B. Stevens, D.E. Stevens, 2003: A large-eddy simulation intercomparison study of shallow cumulus convection. – J. Atmos. Sci. **60**, 1201–1219.

Stevens, B., 2007: On the growth of layers of non-precipitating cumulus convection. – J. Atmos. Sci. **64**, 2916–2931.

Stevens, B., A. Seifert, 2008: Understanding macrophysical outcomes of microphysical choices in simulations of shallow cumulus convection. – J. Meteor. Soc. Japan **86A**, 143–162.

Taylor, C.M., D.J. Parker, P.P. Harris, 2007: An observational case study of mesoscale atmospheric circulations induced by soil moisture. – Geophys. Res. Lett. **34**, L15801. DOI:10.1029/2007GL030572.

Taylor, C.M., A. Gounou, F. Guichard, P.P. Harris, R.J. Ellis, F. Couvreux, M. De Kauwe, 2011: Frequency of Sahelian storm initiation enhanced over mesoscale soil-moisture patterns. –Nature Geosci. **4**, 430–433, DOI: 10.1038//NGEO1173.

Tennekes, H., 1973: A model for the dynamics of the inversion above a convective boundary layer. – J. Atmos. Sci. **30**, 558–567.

van Heerwaarden, C.C., J. Vilà-Guerau de Arellano, A.F. Moene, A.A.M. Holtslag, 2009: Interactions between dry-air entrainment, surface evaporation and convective boundary-layer development. – Quart. J. Roy. Meteor. Soc. **135**, 1277–1291.

van Heerwaarden, C.C., J. Vilà-Guerau de Arellano, A. Gounou, F. Guichard, F. Couvreux, 2010: Understanding the daily cycle of evapotranspiration: A method to quantify the influence of forcings and feedbacks. – J. Hydrometeorol. **11**, 1405–1422.

van Stratum, B.J. H., J. Vilà-Guerau de Arellano, C.C. Heerwaarden, H.G. Ouwersloot, 2014: Subcloud-layer feedbacks driven by the mass flux of shallow cumulus convection over land. – J. Atmos. Sci. **71**, 881–895.

van Zanten, M.C., P.G. Duynkerke, J.W. M. Cuijpers, 1999: Entrainment parameterization in convective boundary layers. – J. Atmos. Sci. **56**, 813–828.

Vilà-Guerau de Arellano, J., 2007: Role of nocturnal turbulence and advection in the formation of shallow cumulus clouds over land. – Quart. J. Roy. Meteor. Soc. **133**, 1615–1627.

Vilà-Guerau de Arellano, J., C.C. van Heerwaarden, J. Lelieveld, 2012: Modelled suppression of boundary-layer clouds by plants in a CO_2-rich atmosphere. – Nature Geoscience **5**, 701–704. Published online September 2nd, 2012; DOI:10.1038/NGEO1554.

Westra, D., G.J. Steeneveld, A.A.M. Holtslag, 2012: Some observational evidence for dry soils supporting enhanced relative humidity at the convective boundary layer top. – J. Hydrometeorol. **13**, 1347–1358.

Wetzel, P.J., S. Argentini, A. Boone, 1996: Role of land surface in controlling daytime cloud amount: Two case studies in the GCIP-SW area. – J. Geophys. Res. **101**, 7359–7370.